Electricity in the Air: Insights From Two Decades of Advanced Control Research and Experimental Flight Testing of Airborne Wind Energy Systems

11 authors, including:

Chris Vermillion
University of North Carolina at Charlotte
94 PUBLICATIONS **733** CITATIONS

SEE PROFILE

Mitchell Cobb
University of North Carolina at Charlotte
14 PUBLICATIONS **66** CITATIONS

SEE PROFILE

Lorenzo Fagiano
Politecnico di Milano
166 PUBLICATIONS **3,787** CITATIONS

SEE PROFILE

Rachel Leuthold
University of Freiburg
17 PUBLICATIONS **90** CITATIONS

SEE PROFILE

Some of the authors of this publication are also working on these related projects:

Thethered Undersea Kite Control View project

Flight dynamics, deformation and aerodynamics of flexible wings for airborne wind energy View project

Graphical Abstract

Electricity in the Air: Insights From Two Decades of Advanced Control Research and Experimental Flight Testing of Airborne Wind Energy Systems

Chris Vermillion, Mitchell Cobb, Lorenzo Fagiano, Rachel Leuthold, Moritz Diehl, Roy S. Smith, Tony A. Wood, Sebastian Rapp, Roland Schmehl, David Olinger, Michael Demetriou

Photographic visualization of a pumping cycle during night operation on 11 October 2018 by tracing a marker light on the kite from the ground station (right) using long-term exposure (courtesy of Kitepower B.V.).

Highlights

Electricity in the Air: Insights From Two Decades of Advanced Control Research and Experimental Flight Testing of Airborne Wind Energy Systems

Chris Vermillion, Mitchell Cobb, Lorenzo Fagiano, Rachel Leuthold, Moritz Diehl, Roy S. Smith, Tony A. Wood, Sebastian Rapp, Roland Schmehl, David Olinger, Michael Demetriou

- This work reviews the progress, in terms of modeling, control design, and experimental prototypes, of the airborne wind energy field over its history, particularly the past two decades.

- The paper provides useful basic formulae for modeling airborne wind energy systems, suitable for researchers and students who are first getting introduced to the field.

- Similarly, the paper introduces readers to the most popular control strategies for airborne wind energy systems, along with descriptions of optimal flight control and modal launch/landing control systems.

- The paper describes the progression of lab-scale and large-scale airborne wind energy system prototypes over the past decade.

- The paper introduces readers to spinoff technology in the marine hydrokinetic energy field, which operates off of the same key principles as airborne wind energy and has the potential to unlock another vast energy resource.

Electricity in the Air: Insights From Two Decades of Advanced Control Research and Experimental Flight Testing of Airborne Wind Energy Systems

Chris Vermillion[a], Mitchell Cobb[a], Lorenzo Fagiano[b], Rachel Leuthold[c], Moritz Diehl[c], Roy S. Smith[d], Tony A. Wood[d], Sebastian Rapp[e], Roland Schmehl[e], David Olinger[f], Michael Demetriou[f]

[a]North Carolina State University, Raleigh, NC, United States
[b]Polytechnic University of Milan, Milan, Italy
[c]University of Freiburg, Freiburg, Germany
[d]ETH, Swiss Federal Institute of Technology in Zurich, Zurich, Switzerland
[e]Delft University of Technology, Delft, Netherlands
[f]Worcester Polytechnic Institute, Worcester, MA, United States

Abstract

Airborne wind energy systems convert wind energy into electricity using tethered flying devices, typically flexible kites or aircraft. Replacing the tower and foundation of conventional wind turbines can substantially reduce the material use and, consequently, the cost of energy, while providing access to wind at higher altitudes. Because the flight operation of tethered devices can be adjusted to a varying wind resource, the energy availability increases in comparison to conventional wind turbines. Ultimately, this represents a rich topic for the study of real-time optimal control strategies that must function robustly in a spatiotemporally varying environment. With all of the opportunities that airborne wind energy systems bring, however, there are also a host of challenges, particularly those relating to robustness in extreme operating conditions and launching/landing the system (especially in the absence of wind). Thus, airborne wind energy systems can be viewed as a control system designer's paradise or nightmare, depending on one's perspective. This survey article explores insights from the development and experimental deployment of control systems for airborne wind energy platforms over approximately the past two decades, highlighting both the optimal control approaches that have been used to extract the maximal amount of power from tethered systems and the robust modal control approaches that have been used to achieve reliable launch, landing, and extreme wind operation. This survey will detail several of the many prototypes that have been deployed over the last decade and will discuss future directions of airborne wind energy technology as well as its nascent adoption in other domains, such as ocean energy.

Keywords: Airborne Wind Energy, Autonomous Flight, Tethered Aircraft

1. Introduction

Over the past three decades, wind energy has evolved from a niche source of energy requiring substantial subsidies, to an established technology delivering more than 590 GW worldwide, which equates to 5% of the global energy portfolio [1]. Furthermore, wind's associated levelized cost of energy (LCOE) has dropped below 4 cents per kWh in many locations. Nevertheless, owing to the geographical variability of ground-level winds, only a small fraction the earth can benefit from such low LCOE from wind. Furthermore, deep-water offshore locations, while often possessing some of the best wind resources on the globe, require a floating platform for economical wind energy harvesting in deep waters, due to the prohibitive tower and installation costs associated with a fixed platform. While significant research and development efforts are focused on economical development of floating offshore wind energy systems,

tethered systems represent a promising long-term solution for fully removing the tower element and associated difficult-to-control dynamics in deep-water sites.

Airborne wind energy (AWE) systems break the above impasse by replacing conventional towered turbines with tethered, flying devices, typically consisting of flexible kites or aircraft [2, 3, 4]. Figure 1 shows several representative examples. For AWE systems, wind is both the source of harvested energy and the means of keeping the devices airborne, via avionic and robotic technologies. Several companies and research organizations have embarked on the design of AWE systems at a variety of scales. Figure 1 illustrates a variety of AWE experimental prototypes. These systems represent four of several dozen prototype AWE systems that have been deployed and in fact reflect key differences that exist between AWE designs today. A classification of AWE concepts is shown in Figure 2. At the highest level, designs are distinguished based on the mechanism of mechanical energy conversion into electricity, which can be done with either a fixed ground station (GS), with a moving (e.g., rotating) ground station, or with generators on board the flying device. The former two types of devices are commonly referred to as *ground-gen* systems, whereas the latter are commonly referred to as *fly-gen* systems. Next, designs are distinguished based on the type of flight motion, which can be either perpendicular to the tether, referred to as *crosswind*, aligned with the tether, or rotational.

Over the past two decades, the AWE community has evolved from a small number of organizations focused on an extremely diverse portfolio of concepts, to a much larger number of organizations focused most dominantly (though not exclusively) on crosswind flight concepts. In particular, some of the most prominent early AWE concepts (some of which are still being pursued either in original form or in variants thereof) included:

- Soft kite designs with ground-based energy conversion, including those of KiteGen [5], SkySails [6], Windlift [7], EnerKite [8], and Kitepower [9]. Although soft kites were arguably the leading design considered in the earlier years of AWE system development, there has been some gravitation away from soft kite designs in recent years, with prominent players such as Windlift [10] and EnerKite [11] now focusing on rigid wing designs.

- Rigid wing designs with on-board generators, which execute crosswind motion. This class of designs was initially explored by Makani Power [12] and is now being continued by both Windlift and KiteKraft [13].

- Rigid wing designs with ground-based energy conversion, which has been adopted by dozens of AWE companies, as detailed in Figure 2 and a similarly wide body of literature in recent years (much of which is detailed in this review paper).

- The X-Wind concept, whereby a group of kite-driven carts are operated on a horizontal closed-loop track on the ground [14].

- Auto-gyro fly-gen concepts developed by institutions such as Sky Windpower and studied in [15].

- Auto-gyro concepts (flying rotors) with tensile torque transfer to the ground and ground-based energy conversion [16, 17, 18].

- Several lighter-than-air concepts, including the EAGLE System project [19] (where cross-flow turbines were suspended from a high-lift aerostat), the Altaeros Buoyant Airborne Turbine (BAT) (where a horizontal-axis turbine was suspended in the central duct of a high-lift shroud [20], the Omnidea airborne module (ABM) (which uses a rotating cylindrical balloon to exploit the Magnus effect for flying pumping cycles) [21], and the Magenn Power Air Rotor System (MARS) (where a Magnus effect aerostat simultaneously served the purposes of lift and power generation). Both the Magenn MARS system and Altaeros BAT have been experimentally demonstrated; however, the MARS system is no longer being pursued, and the Altaeros system is presently being repurposed for telecommunications.

2

A few additional, prominently known AWE system designs have been addressed at a conceptual level but have not been experimentally prototyped. While the community has, at least for the present moment, moved away from these concepts, they have served important roles in the evolution of the AWE community and include:

- The multi-kite LadderMill project designed and developed by the late Dutch astronaut Wubbo Ockels. This patented concept, while serving as the basis for multiple publications, was not ultimately experimentally deployed. It is worth noting, however, that several multi-kite setups are still under consideration in recent literature (see [22, 23, 24, 25, 26]) and through companies such as KiteSwarms.

- The KiteGen carousel concept, whereby a group of soft kites drive a rotary generator on the ground, as introduced in [27], along with several other concepts that focus on driving a rotary generator through multiple airborne kites. To-date, experimental prototyping efforts by KiteGen and others have focused on reel-out/reel-in concepts rather than carousel concepts, whose studies have been limited to conceptual analyses and simulations.

An examination of the aforementioned concepts, along with the timeline along which the concepts were introduced and (where relevant) experimentally prototyped reveals that last decade has seen a gradual transition toward the utilization of crosswind flight, both with airborne and ground-based generation. Due to this trend and the relative dominance of crosswind systems within the AWE control literature, these types of systems will serve as the focus of the technical content in this review article.

Figure 1: Selected AWE systems currently in development: Kitepower, TwingTec, Ampyx Power and Makani Power (from left to right), generating up to 600 kW per single system (photos from [28]).

Among designs that utilize crosswind flight, the majority use a fixed ground station and operate a single device in crosswind flight maneuvers, while reeling the tether from a drum-generator module. For continuous electricity generation, these concepts are operated in pumping cycles, alternating between energy-generating reel-out and energy-consuming reel-in motions of the tether. Maintaining a high tether tension during reel out and a low tether tension during reel in, by discontinuing the crosswind flight maneuvers, results in positive net energy generation per cycle. This operation can be contrasted with the use of small on-board wind turbines, using a conducting tether to transmit the electricity to the ground station. In either power generation mode, the consequence of this crosswind motion is that the flying devices undergo motion that is similar in velocity to the blade tips of a conventional towered system (the blade tips, owing to their greater velocities relative to the blade roots, contribute the vast majority of the power production in conventional towered systems). By replacing the tower and foundation of a wind turbine with a tether/tethers and flying device, AWE systems substantially reduce the amount of material and weight requirements per unit of power. The material savings potential is illustrated in Figure 3. In addition to dramatically reducing material requirements, AWE systems have the capacity to access winds at higher altitudes [30], in addition to offering the ability for altitude adjustment during the course of operation [31, 32, 33, 34].
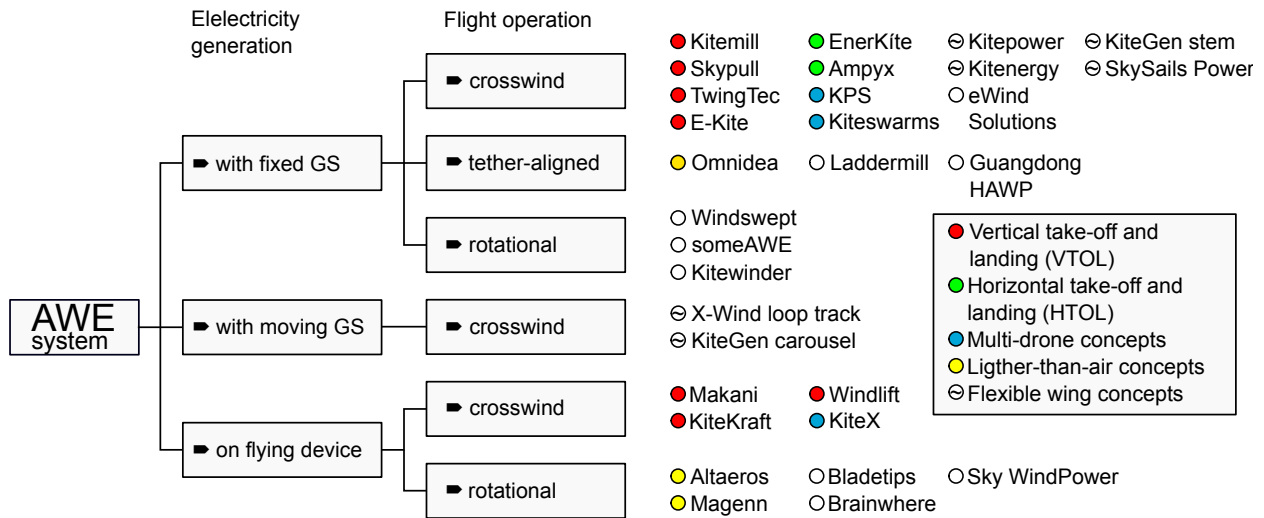
Figure 2: Classification of AWE concepts [29].

While the seminal work of Miles Loyd in [37], along with follow-on work in [38, 39, 40, 41] laid out the framework for describing the underlying mechanics of crosswind flight, the initial work only showed what *could* be achieved with *maximally efficient* crosswind flight. In fact, the development of AWE systems is challenged by complex interdisciplinary interactions, many of which have been largely addressed by the AWE community (the solutions for which are the subject of much of this paper), others of which remain a challenge within the field. Among the first set of tasks that has been addressed by the community is the generation of suitable flight paths and feedback controllers that can successfully navigate these paths under benign wind conditions (e.g., constant winds). A natural next question, which has been the subject of a significant number of studies over the past two decades, surrounds the optimization of the flight path for maximal energy generation, both in constant and variable wind conditions. Another significant topic, which remains an open challenge for the community, is robust control in the presence of wind gusts and other non-ideal atmospheric conditions. In particular, an AWE system's flight speed is strongly coupled with the wind speed and the reeling speed of the tether; this coupling is the root cause of this challenge. Without responsive control, a wind gust can rapidly accelerate the flying device, which amplifies the aerodynamic loads; this leads to potential rupture of the tether or other irreversible damage–and in the worst case, loss of the flying device and/or harm to people. Because aerodynamic control systems are typically too slow to counteract this effect, fault-tolerant winch control, at the physical limits of the actuating electrical drive system, is of critical importance for successful operation of an AWE system. Interlinked with the fundamental problem of tethered flight control are the physics of the wind environment, the aero-elastic response of the flying vehicle and tether, as well as the characteristics of the electrical energy conversion system and the grid integration. Finally, AWE systems must not only robustly execute crosswind flight under non-ideal wind conditions; they also must launch, transition into crosswind flight, execute crosswind flight, transition out of crosswind flight, and land. This modal sequence must be carried out robustly, which is challenging, especially (but not only) for ground-gen systems without on-board rotors for supplemental propulsion.

This paper reviews the literature surrounding the field of AWE system control, which ultimately seeks to address the aforementioned challenges. We begin in Section 2 with a review of the critically important seminal work of Miles Loyd [37] and some more detailed aerodynamic considerations that go into the design of AWE systems. We follow this in Section 3 with a review of dynamic modeling tools for AWE systems, ranging from very simple point mass models to high degree-of-freedom simulation models. This dynamic modeling review is followed in Section 4 by a review of flight control strategies. In Section 5, having introduced control strategies that enable AWE systems to fly prescribed paths at

4

Figure 3: Conventional wind turbines next to docked AWE systems of comparable rated power: photo of the TwingTec pilot system [35] (left) and rendering of the envisioned offshore system of Ampyx Power, the AP4, with a rated power of 2 MW [36] (right).

prescribed altitudes/tether lengths, we turn to optimal control strategies that have been used to maximize the power output of AWE systems in the presence of varying winds and shear profiles. In Section 6, we turn to the critically important question of launching and landing, which has been the subject of an immense amount of literature in the last decade. In Section 7, we review the large collection of experimental platforms that have been designed worldwide, at multiple scales and levels of complexity, all with the unified intentions of validating AWE system and control concepts and de-risking the technology. This discussion focuses on lab-scale platforms developed at the university level, as well as large-scale functional prototypes, including but not limited to the extensive prototyping efforts by Makani Power that have now been publicly disclosed through their "Kite Energy Collection" (including a GitHub code repository [42], flight logs [43], and technical videos [44]). Finally, in Section 8, we examine applications for tethered energy systems that go beyond wind energy; specifically, we examine the use of tethered systems in the less mature field of marine hydrokinetic energy, showing how researchers have leveraged the same fundamental tools to unlock a new source of energy generation underwater. In Section 9, we conclude this paper.

2. Fundamental Principles and Aerodynamic Considerations

To understand the basic mechanics of crosswind flight, we consider the free body diagram of the tethered wing shown in Figure 4. This 2D top-view diagram, which served as the basis for the initial derivations in [37], captures the instant when the tether, which is assumed to be straight, is aligned with the wind velocity $\mathbf{v}_w$. The diagram includes the wind reference frame (x_w, y_w), with its origin $\mathbf{O}$ at the tether anchor point, the x_w-axis pointing downwind, and the y_w-axis pointing in the crosswind direction. The flight velocity $\mathbf{v}_k$ of the device can be decomposed into a crosswind component $\mathbf{v}_{k,y}$ and a wind-aligned component $\mathbf{v}_{k,x}$ due to the reeling of the tether. The relative flow velocity $\mathbf{v}_a$ acting on the lifting device, also denoted as the apparent wind velocity, is given by

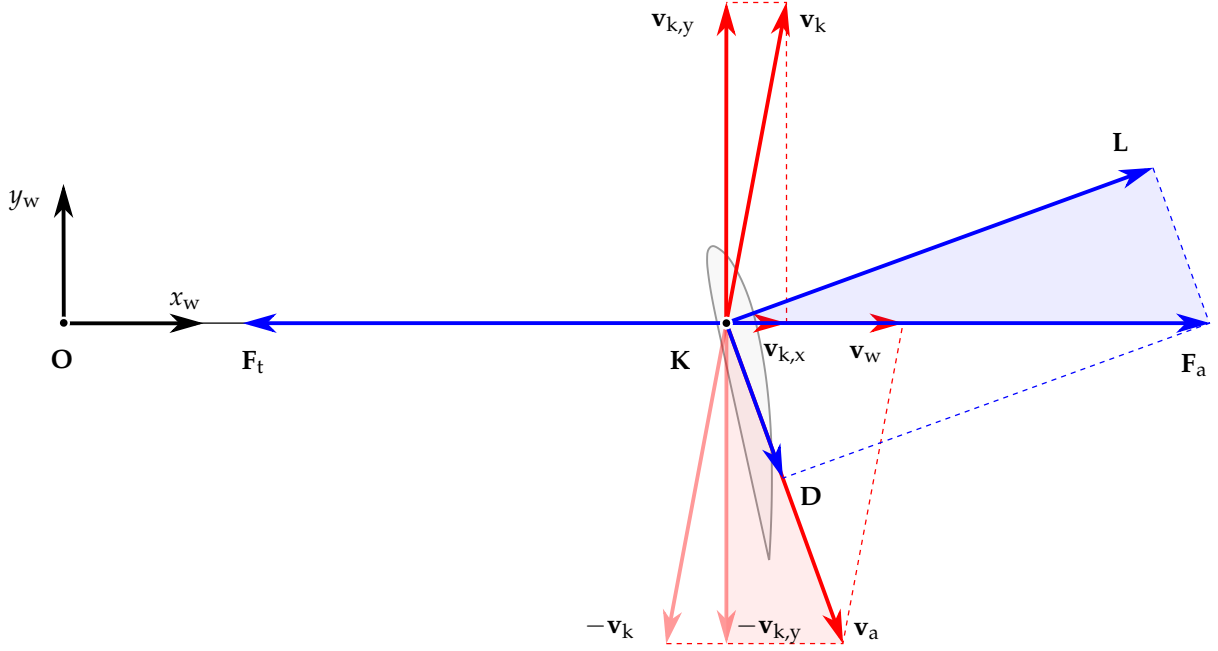$$\mathbf{v}_a = \mathbf{v}_w - \mathbf{v}_k. \tag{1}$$

Figure 4: Basic free body diagram of an AWE system operating in a direct downwind configuration).

In steady flight and neglecting mass, the resultant aerodynamic force $\mathbf{F_a}$ acts in the direction of the tether, balancing the tether force $\mathbf{F_t}$, as any propulsive force component would result in an acceleration or deceleration of the device. Consequently, the triangle formed by the apparent wind velocity $\mathbf{v_a}$, its crosswind component $\mathbf{v_{a,y}} = -\mathbf{v_{k,y}}$ and tether-aligned component $\mathbf{v_{a,x}} = \mathbf{v_w} - \mathbf{v_{k,x}}$ is geometrically similar to the triangle formed by the resultant force $\mathbf{F_a}$, its lift component $\mathbf{L}$ and drag component $\mathbf{D}$. This similarity can be expressed as

$$\frac{v_{k,y}}{v_w - v_{k,x}} = \frac{L}{D},$$

(2)

which leads to a fundamental relationship for crosswind operation:

$$\lambda = E\left(1 - f\right),$$

(3)

where $E = L/D$ is the glide ratio of the device, $\lambda = v_{k,y}/v_w$ the tangential velocity factor, also referred to as the crosswind factor, and $f = v_{k,x}/v_w$ the reeling factor [39]. Equations (1) and (3) can be combined into

$$\frac{v_a}{v_w} = \left(1 - f\right)\sqrt{1 + E^2}.$$

(4)

Based on this simple relationship, we will now examine the power that can be produced under both ground-gen and fly-gen operation.

Ground-gen operation: Under ground-gen operation, mechanical power output is the product of tether force and reeling speed:

$$P = F_t v_{k,x}.$$

(5)

Assuming $F_t = F_a = 1/2\rho S C_R v_a{}^2$, with wing reference area S, resultant force coefficient $C_R = C_L\sqrt{1 + 1/E^2}$ and lift coefficient C_L, we can derive the power harvesting factor $\zeta = P/(P_w S)$ as

$$\zeta = C_L\sqrt{1 + \frac{1}{E^2}}\left(1 + E^2\right)f\left(1 - f\right)^2,$$

(6)

6

where $P_\mathrm{w} = 1/2\rho v_\mathrm{w}^3$ is the wind power density. For wings with high aerodynamic performance, $E \gg 1$, this expression simplifies to

$$\zeta = C_\mathrm{L} E^2 f \left(1 - f\right)^2. \tag{7}$$

The power harvesting factor is maximized for a reeling factor of $f = 1/3$, resulting in an optimal power harvesting factor of

$$\zeta_\mathrm{opt} = \frac{4}{27} C_\mathrm{L} E^2. \tag{8}$$

Fly-gen operation: For fly-gen operation, we distinguish between the drag contributions from the aircraft D_k and the on-board rotors D_r. The mechanical power output is calculated as product of the drag contribution of the rotors and the apparent wind velocity:

$$P = D_\mathrm{r} v_\mathrm{a}. \tag{9}$$

Using the wing reference area S for both D_k and D_r, the aerodynamic coefficients $C_{\mathrm{D,k}}$ and $C_{\mathrm{D,r}}$ can be regarded as non-dimensional additive drag contributions. Combining Equation (9) with Equation (4) for $f = 0$ and $D = D_\mathrm{k} + D_\mathrm{r}$ leads to

$$\zeta = C_{\mathrm{D,r}} \left[1 + \left(\frac{L}{D_\mathrm{k} + D_\mathrm{r}}\right)^2\right]^{\frac{3}{2}}. \tag{10}$$

In his analysis, Loyd showed that a maximum power output is achieved when the rotor drag coefficient is half of the drag coefficient from the aircraft alone. Substituting $C_{\mathrm{D,r}}$ and D_r accordingly leads to

$$\zeta = \frac{1}{2}\frac{C_\mathrm{L}}{E_\mathrm{k}} \left[1 + \left(\frac{2}{3}E_\mathrm{k}\right)^2\right]^{\frac{3}{2}}, \tag{11}$$

where the glide ratio $E_\mathrm{k} = L/D_\mathrm{k}$ is defined without the rotor drag. For $E_\mathrm{k} \gg 1$ this expression further reduces to

$$\zeta_\mathrm{opt} = \frac{4}{27} C_\mathrm{L} E_\mathrm{k}^2. \tag{12}$$

Interestingly, the optimal power production under fly-gen operation has the exact same form as that under ground-gen operation. Examination of these expressions and the derivations thereof gives rise to several important conclusions, listed here for the case where $E \gg 1$:

- Efficient crosswind flight is predicated on the maximization of $C_\mathrm{L} E_k^2$, which, for a given design, is predicated upon flying at an optimized angle of attack.

- For large values of $C_\mathrm{L} E_k^2$, which can approach 100 for a well-designed aircraft, very large amounts of power output are achievable with very little material, i.e. a very small size S of the airborne component.

- From an operational standpoint, flight paths should be chosen that maximize v_a, while the rotor/reeling operation is optimized, and the angle of attack is controlled to maximize $C_\mathrm{L} E_k^2$. Note that in the direct downwind steady flight case, v_a is fully determined by E_k, but when dynamics are involved, this will not always be the case, as the aircraft's position within the wind window and the dynamics of turning flight will come into play.

Though tether drag was not included in the original derivation by Loyd, this important effect can easily be included by modifying the aerodynamic drag coefficient. Due to the fact that the tether's velocity varies along its length (from zero velocity at the anchor point to the velocity of the kite at its attachment point), its drag contribution can be estimated to be equal to the drag resulting from one quarter of the tether length being moved with the same speed as the kite [38, 45, 41].

Another important energy loss in real AWE systems is due to the *cubic cosine losses* resulting from the misalignment of the aerodynamic force with the wind direction. This misalignment is always present to some extent due the tether elevation and system's mass. The analysis of tethered flight can be extended to the full 3D space by means of spherical coordinates, including also the effect of mass, while still assuming a progression through quasi-steady flight states [38, 39]. This generalized theory of tethered flight is validated in [41] using experimental data from a soft kite AWE system operated in automatic pumping cycles up to an altitude of 700 m. From the generalized theory, we can conclude that the available power from Equations (8) and (12) need to be multiplied by the cube of the cosine of the misalignment angle. For example, if the misalignment angle is 30°, only 65% of the power that would be available at perfect alignment, as considered in the analysis above, can be harvested. It is also shown in [41] that for the ideal case of a massless wing that is not actuated, the angle of attack stays constant on any 3D flight trajectory.

A third source of losses that are not included in Loyd's analysis are due to *induction*, i.e., the reduction of the overall wind speed due to the presence of the wind power extracting device. A basic analysis from momentum theory leads to the so-called Betz limit [46], which is reached when the induced wind speed reduction is of a size of $1/3$ of the undisturbed wind. Due to the large size of the swept area of the kite trajectory – typically an annulus or a lemniscate on the spherical surface around the ground station – AWE systems typically lead to lower induction effects than conventional wind turbines. However, induction effects are particularly relevant for the optimization of multiple kite systems [47, 48], and their inclusion into modeling and optimal control of AWE systems is the subject of ongoing research [24, 49, 50].

While unaccounted for based on Loyd's initial quasi-static 2D analysis, the aforementioned losses are accounted for through sufficiently detailed aerodynamic and flight dynamic models, as described in the forthcoming sections. Furthermore, trajectory optimization and control strategies developed over the past two decades and detailed herein can account for these losses. For example, ILC and MPC strategies for optimal flight control, as detailed in Section 5, fully account for cosine losses and also account for tether drag under a sufficiently detailed model.

3. Dynamic Modeling

All of the power output modeling in Section 2 was done under a simplified *steady flight* framework. While this represents a useful starting point, AWE systems exhibit complex 3D dynamics, and achievement of the aforementioned power values requires careful consideration and subsequent control of these dynamics. AWE dynamic models in the literature run the gamut from phenomenological point mass models to high degree-of-freedom models that even take into account such phenomena as wing aero-elasticity (especially prevalent in flexible kite AWE system models).

3.1. The Point Mass Unicycle Model

For the sake of path control design in crosswind flight conditions, a relatively simple model has often proven sufficient and effective. The unicycle model, described e.g. in [51, 52] treats the kite as a point mass that (i) possesses a velocity vector that is governed by quasi-steady flight equations and determines the kite orientation, and (ii) obeys a turning law that has been derived from lateral force equilibrium and validated through a number of experiments. The term "unicycle model" arises from the assumption that the kite obeys a kinematic constraint in which it moves in the direction that it points. This assumption is valid at high apparent wind speeds, as are observed during crosswind flight. In reality, a side-slip angle originates as well; however, its magnitude is small enough to limit the resulting model uncertainty. A crucial feature of the unicycle model is that it uses only three states – two for position on the sphere centered at the ground station with radius r, one for the orientation of the tangential velocity – in contrast to previous point mass models, which used also the velocity magnitude as a state, leading to a four-state system with stiff dynamics [53]. By only considering a kinematic quantity (i.e. the orientation γ of the tangential velocity vector $\mathbf{v}_{k,\tau}$, which is also denoted as course angle) as state and output of the model, the resulting path prediction accuracy has proven to be high for several designs. The model further assumes that the tether is of constant length R and taut; therefore, $\mathbf{v}_k = \mathbf{v}_{k,\tau}$, even though it can be easily extended

to non-vanishing reeling speed. Figure 5, adopted from [54], shows the notation that is used for the unicycle model and the subsequent unifoil model.
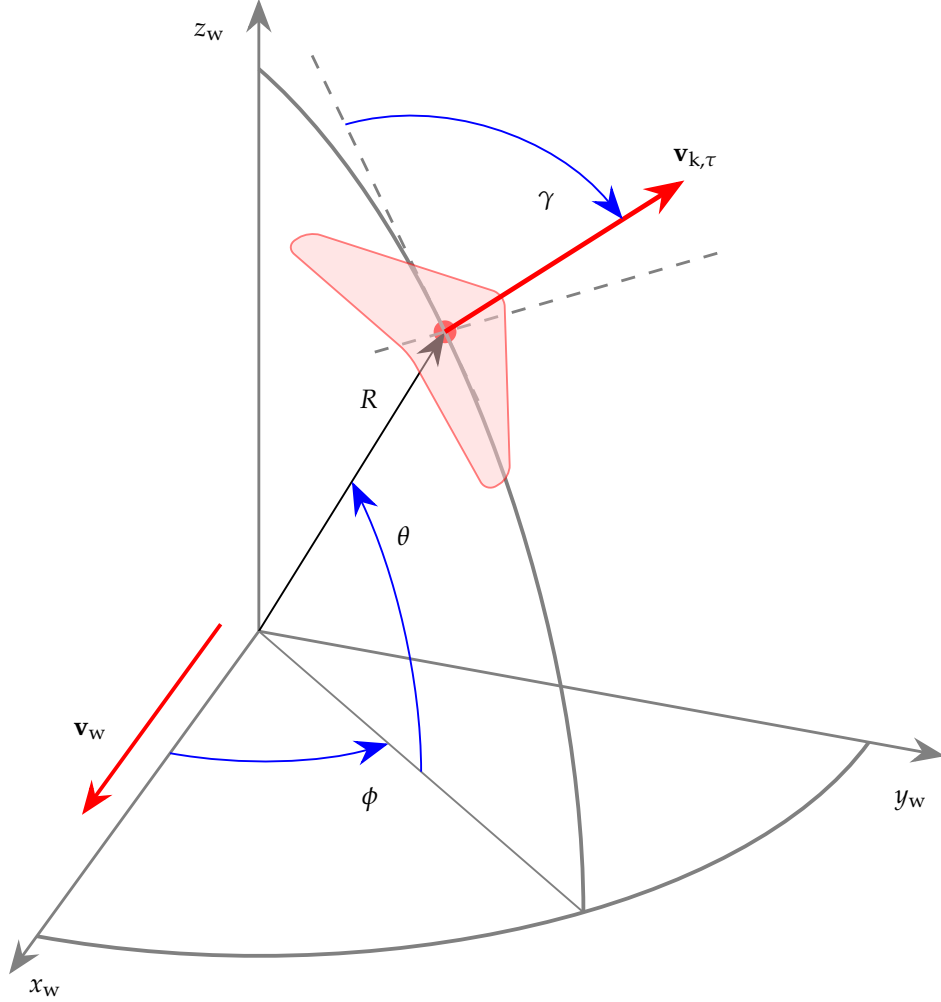

Figure 5: Illustration of the kite kinematics, with elevation angle θ, azimuth angle ϕ, and course angle γ, also denoted as velocity angle, defined as the angle between the tangential kite velocity component $\mathbf{v}_{k,\tau}$ and the zenith on the local tangential plane.

The course angle γ, also referred to as the velocity angle, represents the direction of the kite's velocity vector relative to the zenith, which also represents the heading angle based on the unicycle assumption. For a tether-actuated system, where the control signal, $\delta_s(t)$, is the difference between the port and starboard tether lengths (which induces an aero-elastic twist deformation of the wing and some roll), it has been shown in [51, 55] that the turning dynamics obey

$$\dot{\gamma}(t) = K_s(t)\delta_s(t - \tau_s) + T(t), \tag{13}$$

where the time-varying gain $K_s(t)$ depends on aerodynamic and geometric parameters of the kite and is directly proportional to the apparent speed (see [55] for full details), and τ_s is a steering delay identified in [56]. Examples of experimental validation of this turning law are presented in Figures 6 and 7, in which the steering inputs u and u_s are related to the steering deviation δ_s.

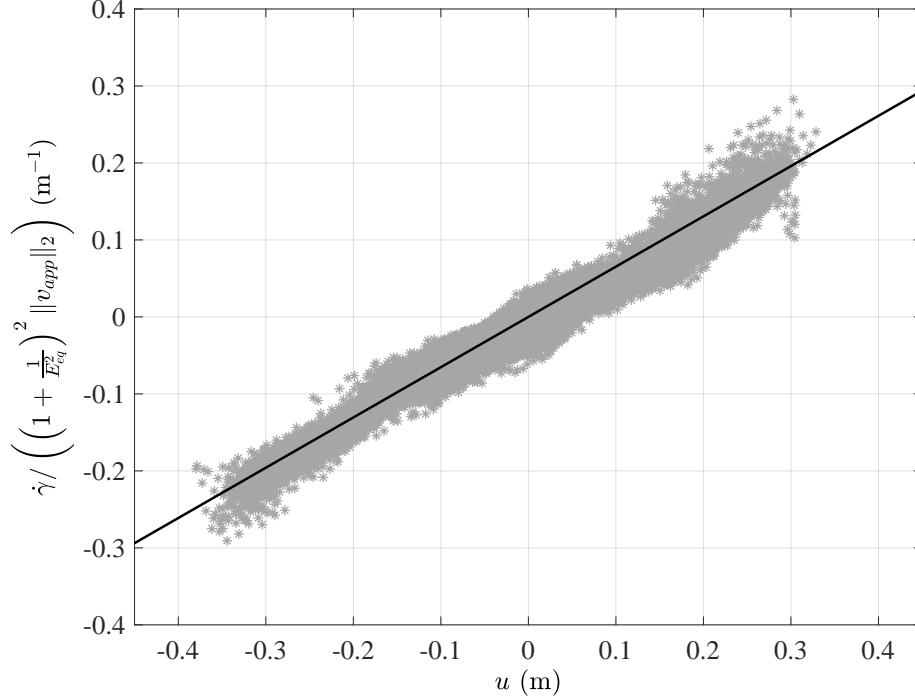Under the unicycle assumption, the kinematics are simply given by:

Figure 6: Experimental validation of the turning law, Equation (13), with a 9 m² power kite. Gray dots: experimental data. Solid line: turning law based on physical considerations and lumped model parameters. Experiments carried out at UC Santa Barbara, see [51].

$$\dot{\theta} \quad = \quad \frac{v_{\mathrm{k}}}{R}\cos\gamma, \tag{14}$$

$$\dot{\phi} \quad = \quad \frac{v_{\mathrm{k}}}{R\cos\theta}\sin\gamma. \tag{15}$$

A key feature of such point mass unicycle models, introduced in [58, 59], is that they use steady flight equations, accounting for the azimuth and elevation angles (i.e., not assuming the kite always to be operating in a direct downwind configuration) to compute the kite's velocity. This results in a kite speed, v_{k}, that can be computed strictly through algebraic equations, where it is derived in [54] (and follows from initial results from Miles Loyd) that:

$$v_{\mathrm{k}} = v_{\mathrm{w}}E\cos\theta\cos\phi. \tag{16}$$

When the kite's apparent speed is small, the variable γ might not be easily measured in practice due to the relatively larger effect of measurement noise. To cope with this issue, a regularized version of the velocity angle has been proposed as well (see [55]), to be used in the absence of on-board heading measurements to replace the velocity angle.

As a matter of fact, the described turning law originates from the centripetal force component contributed by the aerodynamic lift when the aircraft exhibits a roll angle deviation (or a yaw angle deviation,
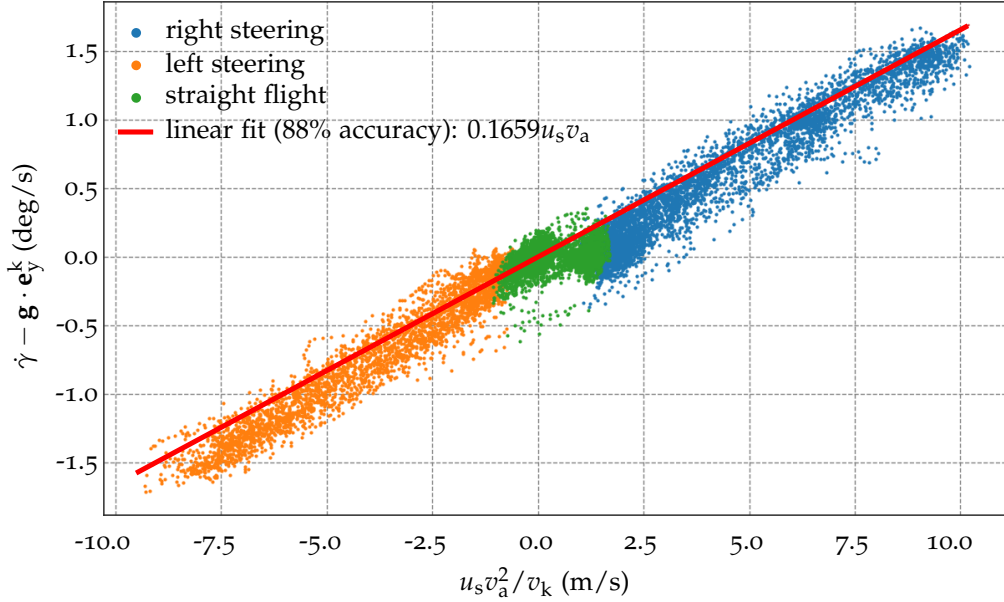
Figure 7: Turning rate law identification using experimental data of a 25 m² kite flying figure-eight maneuvers. The steering input u_s is non-dimendional and can vary between -1 and 1. The data includes 128 individual pumping cycles of a TU Delft V3 kite and was provided by Kitepower B.V. [57].

depending on the employed steering mechanism) with respect to the neutral condition in which the vertical symmetry plane of the kite contains the tether. Based on this observation, a more general version of Equation (13) is readily obtained by considering such a roll angle deviation as an input, see, e.g., [60].

3.2. The Unifoil Model

A compromise between simplicity and consideration of physics-based flight behavior can be attained by retaining the unicycle constraint but replacing the steady flight calculation of v_k with a translational model that accounts for the dynamics of the aircraft (whether a rigid of flexible membrane wing). Furthermore, the phenomenological turning equation can be replaced with a physics-based equation for the yaw moment, which is often more appropriate for rigid wing systems. Because this requires a more detailed aerodynamic and flight dynamic characterization of the lifting body, comprised of airfoils, the resulting model is termed the *unifoil* model. The model is detailed in [61] and is summarized here.

Because the unicycle constraint is preserved, so too are the equations of motion for θ and ϕ. However, the equations for translational motion (in the direction of γ, per the unicycle assumption) and rotational motion are now given by:

$$\dot{v}_k \quad = \quad \frac{1}{m} F_{\text{long}}(\phi, \theta, \gamma, v_f, v_k, \alpha, \beta), \tag{17}$$

$$\ddot{\gamma} \quad = \quad \frac{1}{I} M_{\text{rot}}(\phi, \theta, \gamma, \dot{\gamma}, v_f, v_k, \alpha, \beta) \tag{18}$$

where α and β are the traditionally-defined aerodynamic angle of attack and side slip angles. The expressions for F_{long} and M_{rot} can be quite complicated, as they depend on detailed aerodynamic relationships. Readers are referred to [61] for further details in this regard.

3.3. Higher Degree-of-Freedom Models

In addition to the aforementioned control-oriented models, six degree-of-freedom (6-DOF) rigid body models of the aircraft have been employed, in conjunction with more sophisticated tether models, to

provide higher-fidelity predictions of AWE system behavior. Coupled with more sophisticated tether models and ground station models, the 6-DOF aircraft models can provide rather accurate descriptions of the overall system dynamics. As the sector moves forward towards all-around automation of AWE systems in all operational phases, these models are becoming more and more important. The general form includes the following six ODEs expressed in the body coordinate frame (dependence on the continuous time variable t is omitted for simplicity) and pertaining to angular and linear accelerations [60, 62, 63]:

$$
\begin{aligned}
F_{x_B} &= m(\dot{u} - rv + qw) \\
F_{y_B} &= m(\dot{v} - pw + ur) \\
F_{z_B} &= m(\dot{w} - qu + pv) \\
M_{x_B} &= \dot{p}I_{xx} - (\dot{r} + pq)I_{zx} + rq(I_{zz} - I_{yy}) + q\sum_{j=1}^{4} h_{z,j} \\
M_{y_B} &= \dot{q}I_{yy} + (r^2 + p^2)I_{zx} + pr(I_{xx} - I_{zz}) - p\sum_{j=1}^{4} h_{z,j} \\
M_{z_B} &= \dot{r}I_{zz} - (\dot{p} + qr)I_{zx} + pq(I_{yy} - I_{xx})
\end{aligned}
\tag{19}
$$

where u, v and w are the kite's velocity vector components in the body frame (note that v here represents the body-frame lateral velocity component, which differs from v_k, which represents the total speed of the kite); p, q and r are the rotational speeds around the axes of the body frame; F_{xB}, F_{yB} and F_{zB} are the components of the vector sum of all external forces acting on the kite; finally M_{xb}, M_{yb} and M_{zb} are the components of the vector sum of all external moments. These forces and moments also include the effects of the tether and of on-board actuators (see, for example, [60]). The coefficients $I_{xx}, I_{xx}, I_{xx}, I_{xx}$ are terms in the inertia matrix of the kite; additional ones can be present depending on asymmetries in the design and the position of the center of gravity. For further details regarding higher-fidelity AWE system dynamic models, interested readers are referred to [60, 63, 64, 65, 66].

3.4. Tether and winch models

Because of the distributed aerodynamic drag, gravitational load and inertial effects, the tethers of AWE systems are always exhibiting a certain degree of sag. The approximation as a straight tether is reasonable, when the system is under high load, for example, when harvesting energy in fly-gen operation, or during the traction phases of pumping cycles. However, when retracting the kite, tether sag can have a significant impact on the flight dynamic state of the kite. In the frame of straight-line tether models, the effect of gravity can be taken into account by a correction of the tether force at the ground, while the drag effect can be lumped to the kite [41]. For particular cases, such as kites in static flight, the sagging of the tether can be taken into account by analytical deformation models that are based on the catenary curve [67]. A further improvement of modeling fidelity can be achieved by discretizing the tether with segments. Non-linear spring-mass-damper systems generally follow a straightforward implementation, concentrating the masses of the tether segments at the nodes and using nonlinear springs to model the elastic behavior of the tether material. The nonlinearity stems from the fact that the segments have no compressive resistance. Tether reeling is modeled by either extending or contracting all segments uniformly, or, alternatively, by growing or shrinking the segment closest to the drum, and, if required, removing this segment or adding a new one. This type of models has been applied successfully for different AWE system configurations [63, 68]. To avoid excessively small integration time steps in dynamic simulations, the elastic modulus of the practically very stiff tether material needs to be reduced substantially, which is a source of modeling errors. The other class of discretized tether models is based on rigid or very stiff segments, with masses either concentrated at the segments or distributed to the joints. In [64], on the other hand, the links are modeled as rigid, thereby comprising algebraic constraints and contributing mass. Because this class of models represents the segments as geometric constraints, the time integration can also be challenging, especially when facing transitions from the sagging regime to the elastic stretching regime. The quasi-static tether model presented in [69] neglects transient cable oscillations and longitudinal vibrations, but accounts for the tether elasticity. The approach reduces computational times significantly while maintaining a high resolution of the physics governing tethered flight.

Especially for operation in pumping cycles, the dynamic behavior of the winch is an important aspect of any system model. The winch controls the reeling speed and by that the radial component $v_{k,r}$ of the

kite velocity. Compared to the aerodynamic actuators on the aircraft or kite, the winch a very fast actuator and can be used effectively to compensate wind gusts and turbulent fluctuations. Modelling the winch can be done by combining the differential equations for the inertial system with an expression for the torque-speed characteristics of the generator [68, 66, 60].

4. Control strategies for AWE systems

4.1. Control goals, general control system topology, and operational phases

In the abstract, the two (sometimes conflicting) control goals of an AWE system are identified as maximizing power generation and maintaining safety and reliability during operation [9]. Since AWE systems heavily rely on automatic control to achieve both objectives, and due to the often uncertain and time-varying nature of wind at the time scale of interest for feedback control, the resulting control problem is very demanding. AWE generators are essentially fully autonomous systems [70, 71] that must make safety-critical decisions in an uncertain environment. The challenges of such systems are long-standing in the control and robotics community and have recently gained a renewed interest in the development of control systems in other domains, such as autonomous cars and unmanned aerial systems [72, 73, 74, 75, 76]. A general topology of such autonomous systems, valid also for AWE generators, is presented in Figure 8.
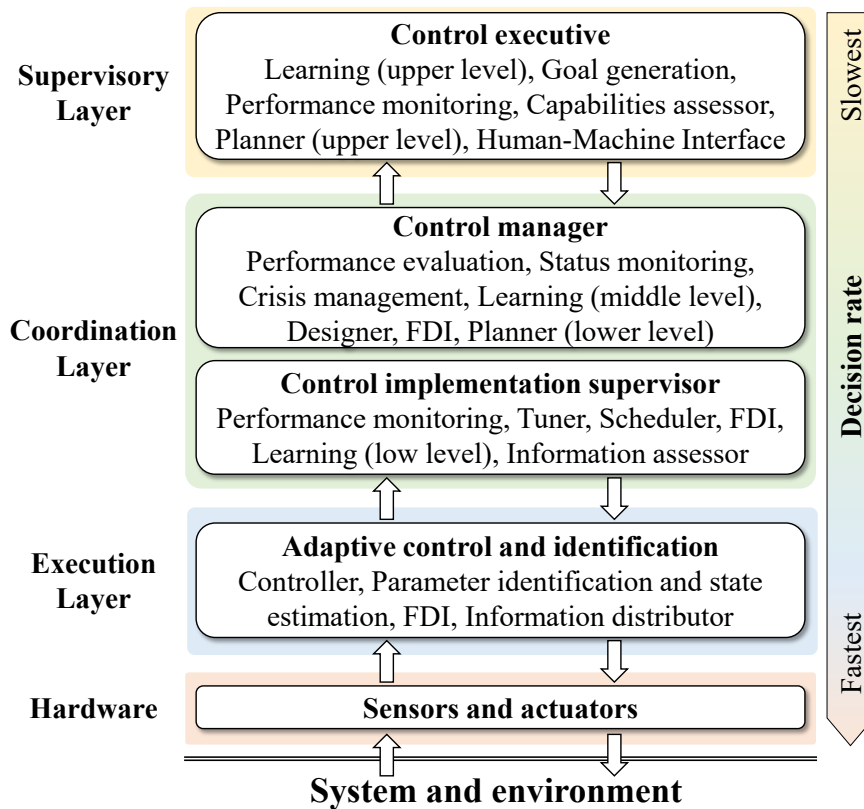

Figure 8: Typical hierarchical structure of autonomous systems such as AWE generators. The layers may feature replicated functions for the various subsystems, e.g., kite and ground station. Adapted from [70].

In normal (i.e. non-faulty) operating conditions, the system must manage the following distinct operational phases and the transitions among them (see, e.g., [60]):

- **Launch**. This refers to the take-off maneuver, performed when wind conditions are suitable, that ultimately brings the AWE system to its operating altitude.

- **Power generation**. The system transitions to dynamic flight and begins harvesting energy, either through pumping operation or in drag power operation, depending on the specific layout. In pumping operation, power generation is further divided into traction and retraction sub-phases, along with suitable transitions.

- **Landing**. When wind conditions are not suitable to generate energy (either too little or wind or excessively strong wind), the system initiates this phase, which culminates in the retrieval and storage of the aircraft until the next take-off.

As the operational phases differ significantly in terms of operating conditions and control sub-goals, different control strategies are employed in each phase, and a supervisory logic structure is in charge of switching among phases and thus among such control strategies, ensuring that the ground station control and on-board control cooperate. A representative high-level supervisory control schematic is shown in Figure 9, from [60]. In the literature, most contributions are focused on crosswind flight control and on
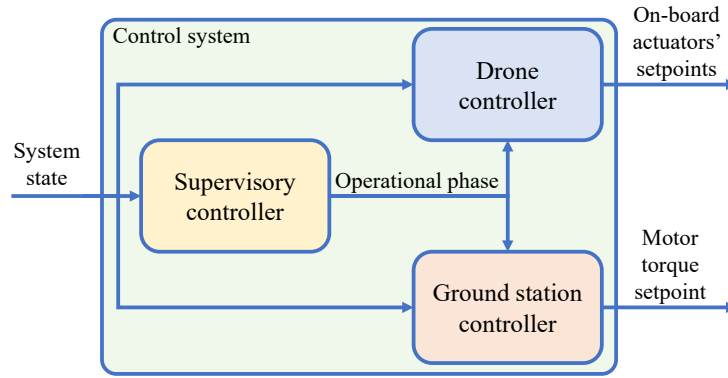

Figure 9: Example of layout of the supervisory control logic for an AWE system.

pumping operation. These aspects are described in the next sub-section, with optimal control strategies described in Section 5. A smaller number of contributions deal instead with take-off and landing phases and with all-around automatic control. These are described in Section 6.

4.2. Control strategies for crosswind flight and pumping operation

To derive the control laws for a hierarchical control approach, the dynamics of the aircraft are divided into slow (outer loop) and fast (inner loop) dynamics. In the outermost loop, the *Guidance Module Traction/Retraction* calculates the desired direction for intercepting and following a prescribed flight path. In AWE systems, the reference flight path during the traction phase is in general given by either a figure-eight or circular/elliptical path, whereas the reference flight path for retraction is often a simple straight line. For the figure-eight path, a continuous Lemniscate parameterization is chosen (see [77, 78, 79, 80, 81]) as the reference, which can also be discretized to obtain a fixed number of waypoints along the path (see [59, 82]). Other approaches further abstract the path-following problem and use waypoints and switching logic instead (for instance [83]). In all of these approaches, either a reference point on the path or the current active waypoint needs to be determined, which then makes it possible to calculate a desired flight direction. The overview architecture in Figure 10 assumes a Lemniscate parameterization given in Cartesian coordinates by $\mathbf{\Gamma}_t(s)$. In that case, a point on the path is defined by the path variable $s \in [0, 2\pi]$. In this example, the desired point on the path is defined as the closet point on the path with respect to the current aircraft position. Based on the desired directional angles, usually denoted as the kinematic (k) course $\chi_{k,set}$ and flight path angle $\gamma_{k,set}$, the corresponding course rate $\dot{\chi}_{k,set}$ and path angle rates $\dot{\gamma}_{k,set}$ are calculated, thereby linking the guidance loop output with the aircraft point-mass flight dynamics. In [79], these rates are directly calculated based on the curvature of the flight path during the traction phase,
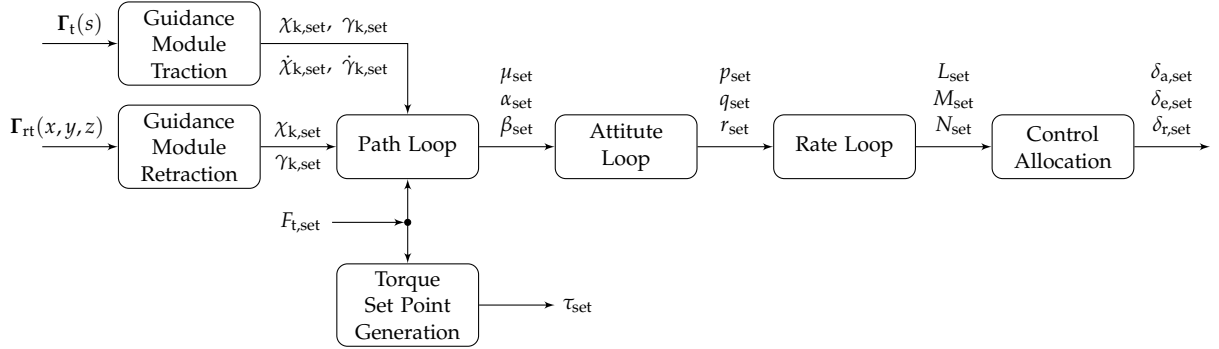
Figure 10: Cascaded control structure of flight and winch control system for traction and retraction mode. Feedback paths are omitted in the figure.

in combination with a proportional feedback on the deviation between the actual course/path angle and reference course/path angle. Another option is to calculate these rates through a reference filter, also in combination with an error feedback term. In [79], the latter approach is taken for the straight path ($\mathbf{\Gamma}_{rt}(x, y, z)$ in Figure 10) following in the retraction phase.

To calculate the output of the *Path Loop*, the point-mass dynamics of the aircraft can be written in terms of the course and flight path rate, i.e.,

$$
\begin{aligned}
\dot{\chi}_k &= \frac{1}{m_a \cos \gamma_k v_k} \left(f_{y,m} + f_{t,y,K} \right) \\
\dot{\gamma}_k &= \frac{1}{m_a v_k} \left(f_{z,m} - \cos \gamma_k m_a g - f_{t,z,K} \right)
\end{aligned}
\tag{20}
$$

where m_a is the aircraft mass, v_k is the speed of the aircraft, g is the gravitational constant, and $f_{t,y,K}$ and $f_{t,z,K}$ are the tether force components in the kinematic frame K (see [79]). Setting the course rate and path angle rates equal to the desired rates coming from the guidance loop makes it possible to solve for the required maneuver forces, $f_{y,m}$ and $f_{z,m}$. The set points for the bank angle and lift coefficient can then be approximated by

$$
\begin{aligned}
\mu_{set} &= \arctan \left(\frac{f_{y,m}}{f_{z,m}} \right) \\
C_{L,set} &= \frac{\sqrt{f_{y,m}^2 + f_{z,m}^2}}{0.5 \rho v_a^2 S_w}.
\end{aligned}
\tag{21}
$$

The angle of attack set point for the attitude loop is then calculated by inverting the lift coefficient. In the linear regime this yields

$$
\alpha_{set} = \frac{C_{L,set} - C_{L,0}}{C_{L,\alpha}}.
\tag{22}
$$

The attitude angle that defines the directional orientation is in this case given by the side slip angle, β, and the corresponding set point is set to zero. It is worth noting that, besides the additional term represented by the tether force, this strategy is originally proposed in [84] for un-tethered aircraft. Note that it is crucial here to use the set point for the tether force if Equation (20) is inverted. This can be achieved by using a straight line approximation for the tether. The tether force set point components are then given by

$$
\begin{pmatrix} f_{t,x,K} \\ f_{t,y,K} \\ f_{t,z,K} \end{pmatrix} = -\mathbf{M}_{KW} \left(\frac{\mathbf{p}_W}{\|\mathbf{p}_W\|_2} F_{t,set} \right)
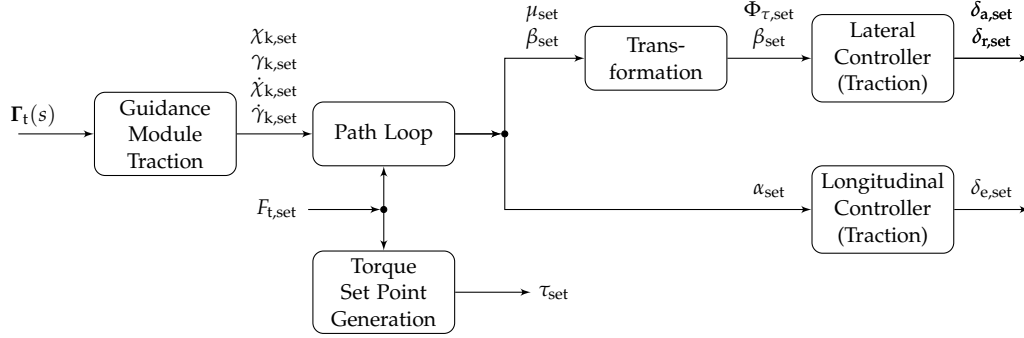\tag{23}
$$

15

Figure 11: Cascaded control structure of flight and winch control system for the traction mode including a decoupled state feedback controller. Feedback paths are omitted in the figure.

where $\mathbf{p}_W$ is the position of the aircraft in the Wind frame and $F_{t,set}$ is the tether tension set point. The matrix $\mathbf{M}_{KW}$ transforms a vector from the W frame into the K frame (see [79]). This makes it possible to implicitly use the aircraft in combination with the winch to control the tension in the tether. On the aircraft level, the lift force magnitude and orientation is adapted through μ_{set} and α_{set} to compute the desired tension in addition to the required maneuvering force to follow the path. This also has the benefit of allowing the tension in the tether to be quickly reduced by the flight controller in case of a predicted tether rupture, even if the winch reeling speed or acceleration is saturated. On the winch level, the tether force is controlled by adapting the reeling in/out speed. The reeling speed is adapted according to the torque set point τ_{set}, which can be calculated based on a proportional-integral tether force tracking error feedback.

4.2.1. Linear Inner Loop

Although the figure-eight flight maneuvers are nonlinear, it is possible to derive linear state feedback controllers that can track the outer-loop commands. This can be achieved through an appropriate choice of state feedback variables and an attitude parameterization with respect to the tangential plane. Because the attitude angles vary less with respect to the tangential plan than the ground, this attitude parameterization with respect to the tangent plane allows for the relatively straightforward design of linear feedback control laws [82]. The state-space models are obtained through a linearization of the six degree of freedom aircraft dynamics around the figure-eight path where the tether force is regarded as an additional input. Trim points are calculated as usual by requiring all accelerations to be zero. As an additional constraint, the course and path angle rates are set to the corresponding rates that are calculated based on the path curvature, and the tether force is set to the traction phase set point. Furthermore, the linear state space models can be decoupled into longitudinal and lateral dynamics, analogously to conventional linear flight control system design. The corresponding architecture is displayed in Figure 11. The linear inner loop for the retraction phase is constructed similarly. Since the retraction phase resembles a glide path, the attitude can be parameterized with respect to the ground. Note that this yields a set of four controllers, requiring the switching of the inner-loop controller when switching from traction to retraction phase and vice versa. The longitudinal traction phase inner-loop controller can be designed using the state space model defined by

$$
\begin{pmatrix} \dot{v}_a \\ \dot{\alpha} \\ \dot{\Theta}_\tau \\ \dot{q} \end{pmatrix} = \mathbf{A}_{lo,t} \begin{pmatrix} v_a \\ \alpha \\ \Theta_\tau \\ q \end{pmatrix} + \mathbf{B}_{lo,t,1} \delta_e + \mathbf{B}_{lo,t,2} F_t. \tag{24}
$$

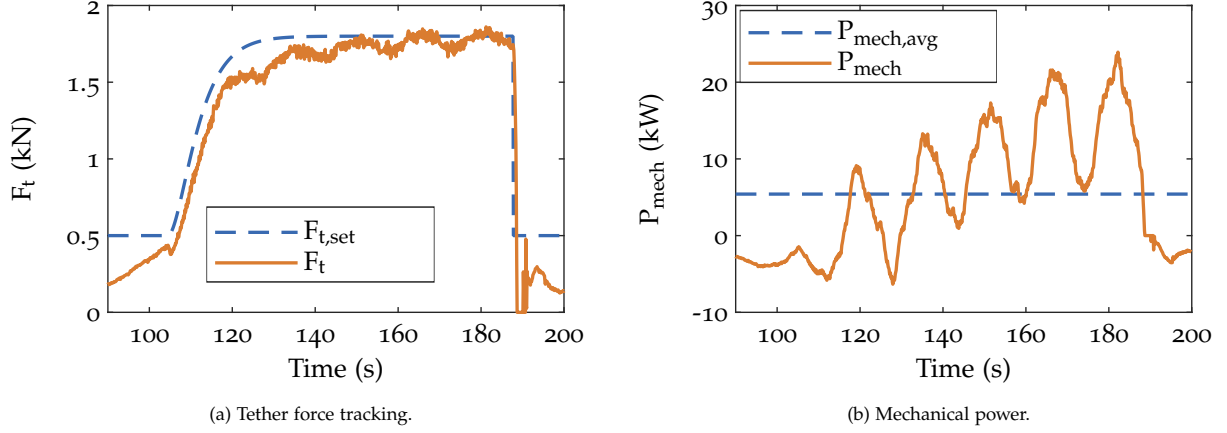(a) Tether force tracking.   (b) Mechanical power.

Figure 12: Linear control performance during one pumping cycle in turbulent wind condition (see Figure 11).

The state space model for the lateral traction phase controller design is given by

$$
\begin{pmatrix} \dot{\beta} \\ \dot{\Phi}_\tau \\ \dot{p} \\ \dot{r} \end{pmatrix} = \mathbf{A}_{\text{lat,t}} \begin{pmatrix} \beta \\ \Phi_\tau \\ p \\ r \end{pmatrix} + \mathbf{B}_{\text{lat,t,1}} \begin{pmatrix} \delta_a \\ \delta_r \end{pmatrix} + \mathbf{B}_{\text{lat,t,2}} F_t.
\tag{25}
$$

The state space models for the retraction phase are constructed analogously. However, due to the different attitude parameterization, the attitude angles with respect to the tangential plane, Φ_τ and Θ_τ, need to be replaced with the conventional attitude parameterization with respect to the ground, Φ and Θ. As is standard, all states and inputs are defined with respect to the trim states. In both cases, a kinematic transformation from the bank angle command ($\Phi_{\tau,\text{set}}$) to the corresponding roll angle (Φ) is required, as indicated by the *Transformation* block in Figure 11. With these state space models, many different linear control strategies can be applied. The following results are obtained using an LQR state feedback design with an additional integral error feedback part to track the path loop commands. In this case, the state space models need to be augmented with additional integral error states for the gain synthesis. To avoid the need for gain scheduling, the controller is designed such that it ensures stability and sufficient robustness margins simultaneously at different trim points. The control laws for the traction phase are then given by

$$
\delta_{e,\text{set}} = -\mathbf{K}_{\text{lo,t}} \begin{pmatrix} \mathbf{x}_{\text{lo,t}} \\ \int_0^t (\alpha_{\text{set}} - \alpha)\, d\bar{t} \end{pmatrix}
\tag{26}
$$

$$
\begin{pmatrix} \delta_{a,\text{set}} \\ \delta_{r,\text{set}} \end{pmatrix} = -\mathbf{K}_{\text{lat,t}} \begin{pmatrix} \mathbf{x}_{\text{lat,t}} \\ \int_0^t (\Phi_{\tau,\text{set}} - \Phi_\tau)\, d\bar{t} \\ \int_0^t (\beta_{\text{set}} - \beta)\, d\bar{t} \end{pmatrix},
\tag{27}
$$

where $\mathbf{x}_{\text{lo,t}}$ and $\mathbf{x}_{\text{lat,t}}$ are the state vectors for the traction phase as defined in Equation (24) and Equation (25), respectively. The control laws for the retraction phase have the exact same structure, only with the aforementioned differences in the state vectors. Representative flight performance results under the aforementioned controller are shown in Figures 12a-14b.

4.2.2. Nonlinear Inner Loop

The inner loop can also be realized as a nonlinear controller. In this case, the set points calculated in Equation (21) and Equation (22) are passed to the *Attitude Loop* and *Rate Loop*, which control the attitude
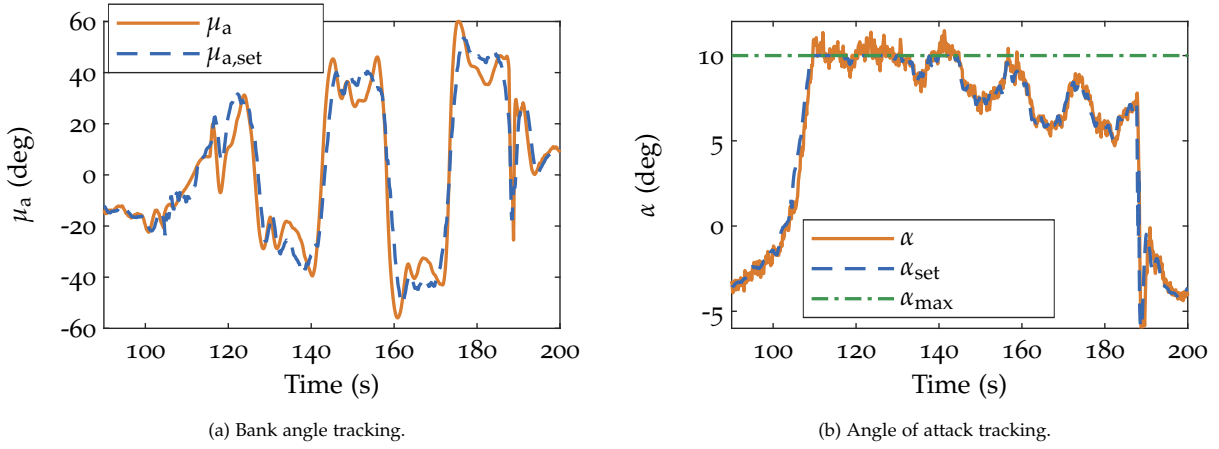
17

(a) Bank angle tracking.

(b) Angle of attack tracking.

Figure 13: Linear inner loop control performance during one pumping cycle in turbulent wind condition (see Figure 11). Note that α_{max} represents a saturation limit on the angle of attack setpoint.

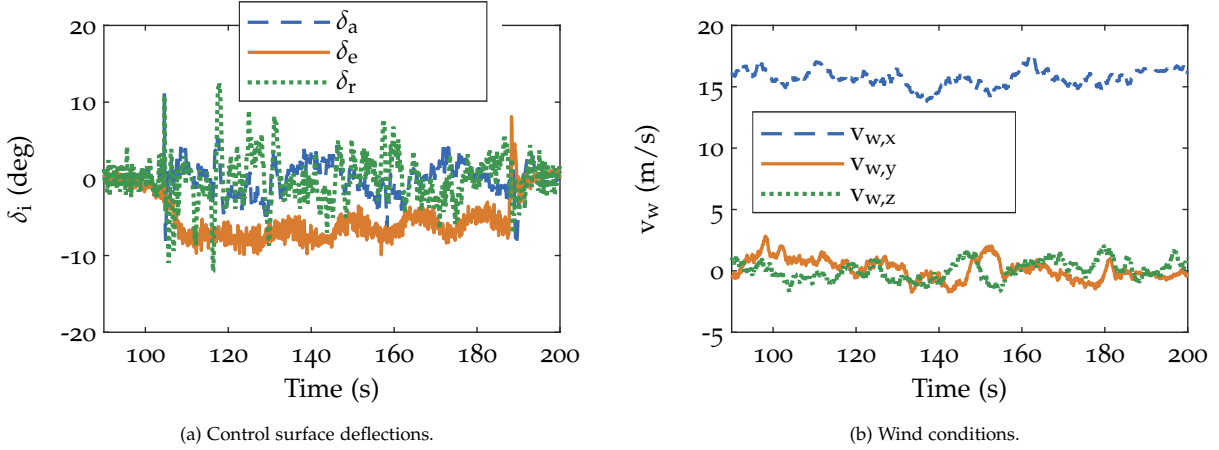(a) Control surface deflections.

(b) Wind conditions.

Figure 14: Actuator outputs using the linear inner loop controller (see Figure 11) in a turbulent wind field .

and rigid body rates. In the last step, the control output is allocated to the actuators (termed *Control Allocation*) . One approach to achieve this task is presented in [79], using nonlinear dynamic inversion (NDI). Corresponding rates for the bank and angle of attack are calculated using second-order reference filters in addition to a proportional error feedback part. Using kinematic relations, the resulting rates are transformed into the conventional rigid body rotational rates consisting of roll rate p_{set}, pitch rate q_{set}, and yaw rate r_{set}. Inverting the rotational dynamics and linearizing the nonlinear aerodynamic moment equation makes it possible to allocate moment increments to actuator deflection increments, which are then added to the current actuator deflection to yield the desired aileron, elevator and rudder deflections, $\delta_{\mathrm{a,set}}$, $\delta_{\mathrm{e,set}}$ and $\delta_{\mathrm{r,set}}$, respectively. The advantage of the nonlinear inner loop is that the same controller can be used for the traction and retraction phase. As a result, this approach only needs to switch the guidance mode from figure-eight path-following on a sphere (traction phase) to straight line following (retraction phase), and vice versa.

4.2.3. Other approaches for path control and pumping operation

In the literature, most approaches share variants of the cascade control structure presented in the previous sections, which sometimes differ in the subtleties of how one or more of the layers are designed. Different guidance strategies for dealing with time-varying uncertainties have been derived, e.g. in [85,
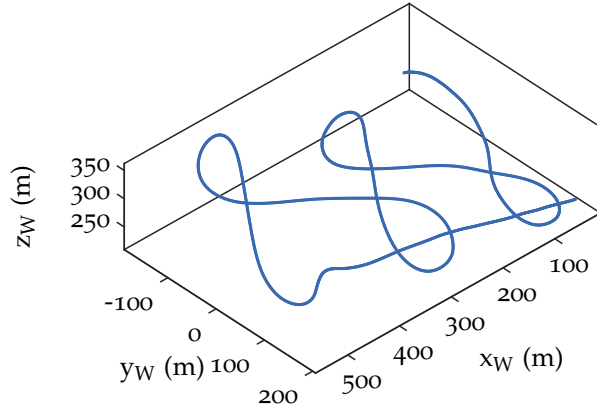
Figure 15: Pumping cycle trajectory using the linear inner loop (see Figure 11)

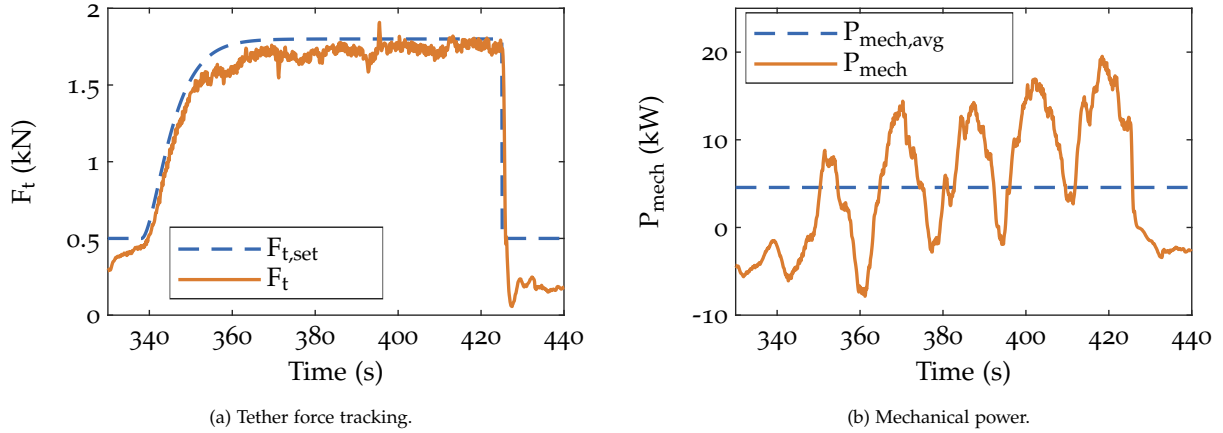

(a) Tether force tracking.

(b) Mechanical power.

Figure 16: NDI control performance during one pumping cycle in turbulent wind condition (see Figure 10).

86, 87]. In [54, 81, 88], path following control approaches with compensation for actuation delay were introduced. Furthermore, different approaches for the path control layer have been proposed and tested either experimentally or in simulation with detailed models. A family of approaches, employed in [51, 52, 55, 58, 89, 90, 91, 92], utilize pre-defined target points, sometimes adjusted in real-time for the sake of performance optimization, by an upper control layer (see e.g. [93]). At each control time step, the current position of the kite and the position of the active target point are used to compute a reference velocity angle, which is then given to a linear feedback controller that manipulates the steering input (or the kite attitude) in order to track it. Switching among target points is carried out when suitable proximity conditions are met. These approaches proved to be very effective and robust, at the cost of losing a direct link to the resulting path's shape. Target point strategies have been successfully employed also in combination with adaptive techniques [89], in the retraction phase of pumping operation [55], as well as during take-off and landing with different types of systems (see [90] and Section 6).

Reference [94] presents a methodology for augmenting an existing baseline controller with a prediction and prevention methodology to improve the resilience of the controller against external disturbances caused by varying wind conditions. In a first step, upset conditions are systematically generated in which the given controller is no longer able to achieve its objectives. The generated knowledge is then used to synthesize a model that predicts upsets beforehand, which allows triggering avoidance maneuvers.

(a) Bank angle tracking.
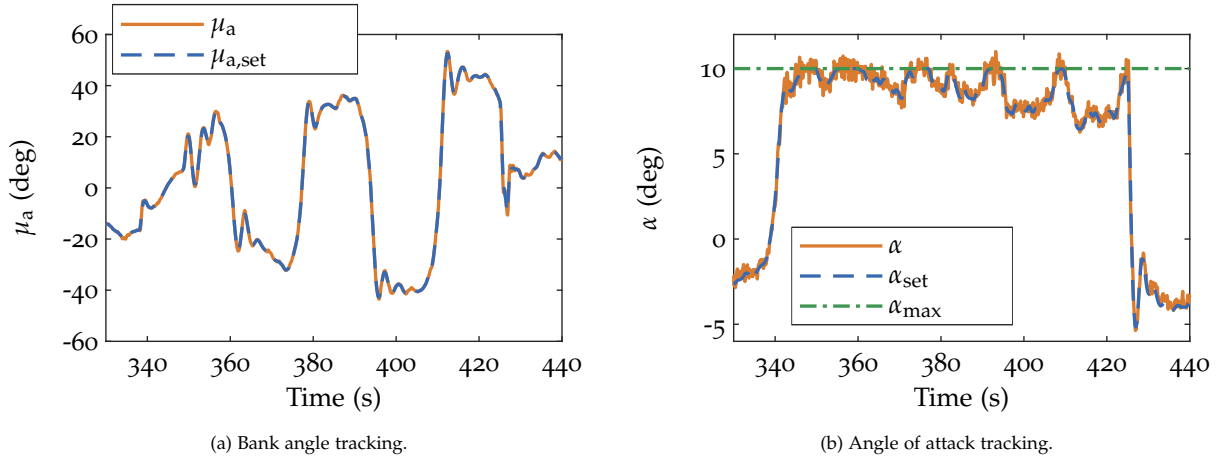

(b) Angle of attack tracking.

Figure 17: NDI control performance during one pumping cycle in turbulent wind condition (see Figure 10). Note that $\alpha_{\max}$ represents a saturation limit on the angle of attack setpoint.
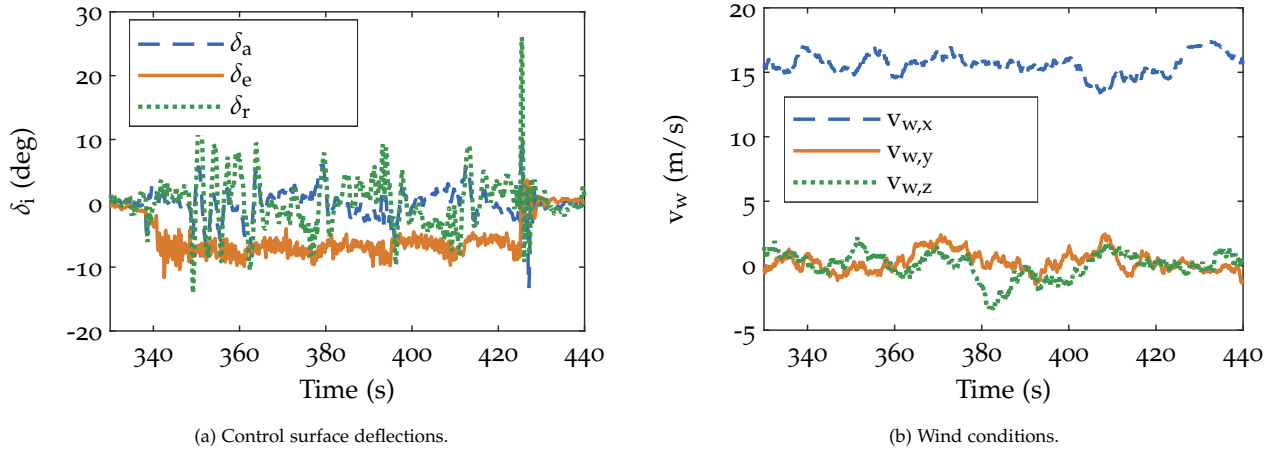

(a) Control surface deflections.

(b) Wind conditions.

Figure 18: Actuator outputs and turbulent wind field obtained with the NDI controller (see Figure 10).

4.2.4. *Winch/ground station control systems*

For maximum power generation, for a given reel-out speed, the tension in the tether should be maximized, subject to structural limits, during the traction phase. Large overshoots need to be avoided in order to prevent force peaks that exceed the maximum tensile force the tether and the aircraft structure can still support. During the retraction phase, a significantly lower tension needs to be tracked in order to reduce the amount of consumed power while reeling in. Simultaneously, tether sag needs to be minimized. Similarly, during take-off and landing, coordination between the aircraft and the winch is required to minimize tether sag and power consumption.

One simple approach to solve this task is to calculate the winch torque based on a proportional-integral feedback driven by the difference between the measured tether force at the ground station and the tether force set point. In that case, the winch accelerates (reeling out faster) if the measured force is larger than the set point and decelerates (reeling out more slowly) if the tether force is below the set point. Results of this approach are depicted in Figures 12a and 16a. Reference [60] provides explicit details on how the tether force set point should be selected for traction, recovery, and low-tension phases of operation.
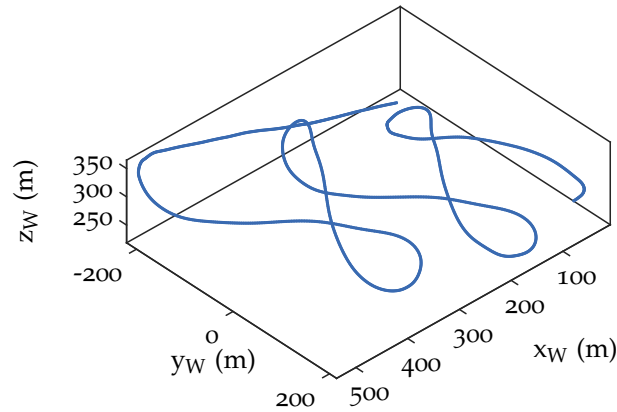
20

Figure 19: Pumping cycle trajectory using the NDI inner loop (see Figure 10)

4.3. State and parameter measurement and estimation

In the description of control approaches provided so far, an underlying assumption is that the relevant feedback quantities and required model parameters are available. In practice, this is achieved by means of observers to estimate unmeasured states and parameters and to reduce the effects of measurement noise. In the literature, several approaches have been proposed [95, 96]. The basis of these approaches is to employ state-of-the-art algorithms for inertial measurement and estimation, exploiting accelerometers, magnetometers, gyroscopes, and GPS. Tether angle and tether force readings are also commonly employed. Alternative dedicated sensors based on range measurements [97] and visual motion tracking [98] have been considered. Several works also exploit specific features of AWE systems to achieve improvements over standard estimation techniques, in particular by taking into account the constraint provided by the tether [99].

5. Optimal Control Strategies

One of the most important aspects of AWE system control involves the development of algorithms that maximize power output, so as to realize performance levels as close to Loyd's theoretical limits as possible while respecting a multitude of constraints. Several techniques have been proposed in the literature for doing this, involving offline optimal control, model predictive control (MPC), and online adaptive control techniques such as extremum seeking (ES) and economic iterative learning control (ILC). In this section, we will review each of these techniques, as they apply to AWE systems.

5.1. Offline Optimal Control for Performance Prediction

Offline optimal control has made the prediction of an AWE system's performance – in terms of power production (see Figure 20), levelized cost of energy (LCOE), and AWE's role in the energy market – much more methodical over the last decade.

5.1.1. Optimal Control Problems

Any optimization problem will sweep over some decision variables, considering only those sets of values that satisfy specified constraints, in order to find the smallest value of some cost function (or largest value of some reward function). In an optimal control problem (OCP), the decision variables define the concrete system behavior, which must be consistent with the modeled system dynamics – among other constraints – over the entire optimization period. An AWE OCP can seek to maximize the average system power [23, 25, 45, 101, 102, 103]; maximize the total energy generation [104, 105, 106]; reward robustness on safety-critical constraints [86, 107, 108]; or meet some other target. Detailed information about numerical methods for the solution of OCPs can be found in [109, 110] or in [111, Chapter 8].
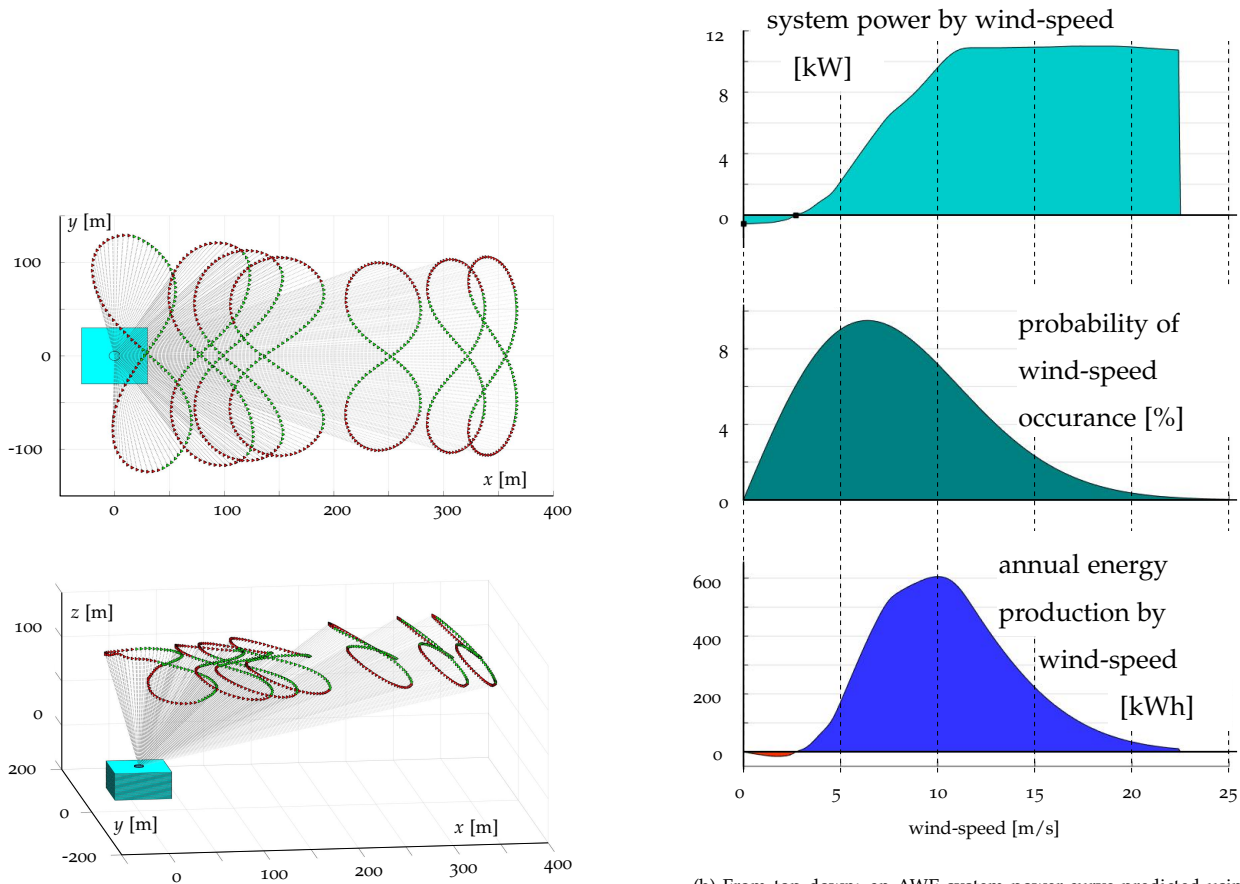
(a) Top- and side-views of optimal trajectories at different reference wind speeds. Green markers depict power-generating (reel-out) portions of the trajectory; red markers depict power-consuming (reel-in) portions of the trajectory.

(b) From top down: an AWE system power-curve predicted using optimal control; the probability density function for the reference wind speed at a site; the total energy that the AWE system is predicted to generate for one year, with net operational power (orange) consumption and (blue) generation.

Figure 20: An example of the AWE system performance predictions that can be made using offline optimal control. These figures are reproduced from [100].

5.1.2. Examples of AWE Performance Predictions Available Through Optimal Control

Optimal control is a particularly powerful tool, which can be used to make predictions ranging from situation-specific system responses to the role of AWE in the larger energy market.

Optimal control can predict how an AWE system should behave in specific situations, such as launching and landing (e.g., [22] and [112]). Further, the observation that the optimal average power may be negative motivates specific strategies [100, 113] for remaining aloft at low wind speeds. Once it became possible to predict what an AWE system should do at any particular wind speed, it became possible to construct power curves for AWE systems. Using an OCP-generated power curve and statistical wind characteristics, a system's annual energy production (see [100] and Figure 20), and capacity factor (see [114]) can be found for particular sites. Further, measurements of the wind velocity profile at a particular site can be processed with k-means clustering and entered into an OCP to predict how the system power will vary in time [115, 116].

In its most complex incarnation, optimal control can be used to predict kite farm performance and the role of AWE in the energy market. The work of [117] uses OCP-generated operational characteristics to predict the LCOE of specific kite-farm layouts. Then, [118] estimates the loss in power that might result from constraining a farm's kites to fly phase-shifted versions of a single trajectory (as a supply-side

energy management strategy) rather than allowing the kites to fly individually optimal trajectories. The work of [119] considers the value of AWE system-generated energy in a mixed energy portfolio, and specifically finds high value in systems with low cut-in speeds, as well as (separately) sites with strong wind shear. Further, [120] predicts the marginal cost of additional AWE capacity, for regions with specific wind resources when an arbitrary amount of AWE capacity is already installed.

Various open-source toolboxes can simplify the formulation and solution of such problems. These include CasADi [121], the open Optimal Control Library openOCL [122], LAgrangian Kite Simulators LAKSA [123], and the awebox [124].

5.1.3. Some Open Modeling Questions in AWE Optimal Control

OCP-based power predictions were compared to real-world experimental values in [103]. Several real-world effects were identified as resulting in overly optimistic OCP predictions, including controller performance limits, communication delays, model-plant mismatch with respect to the wind field, kite aerodynamics, and tether behavior. Model-plant mismatch problems can be addressed via robustness [101, 108] or through further work in model development/selection. Ultimately, OCP-generated performance predictions can only be as accurate as the models that make up the OCP constraints.

Since tether drag and stress prevent an optimizer from simply preferring infinitely large kites and infinitely fast flight speeds, appropriate tether model selection is a serious issue for AWE OCPs. For example, [100] specifically notes that performance predictions are highly sensitive to the applied tether drag model. For the sake of simplicity, many OCPs, e.g., [25, 48, 119], model tethers as in-elastic, tensioned rods. This avoids the stiff dynamics that arise from elasticity and enables a straightforward tether drag estimation using known cylindrical-body coefficients. However, the modeling of tether sag requires many tether elements, which tends to inflate the OCP problem size. The quasi-steady tether model used by [112] does model tether sag and elasticity, but is not well suited to modeling crosswind situations. To date, the impact of local tether behavior (e.g., rotations and vibrations) on AWE OCPs has not yet been studied.

Conservation of momentum in the flow field is the main reason that wind energy systems are not able to perfectly convert the wind's kinetic energy into generated energy. When this physical phenomenon, abbreviated as the induction effect, is not included in AWE OCPs, the conversion efficiency does tend towards unity, as in [45]. However, when [49] flies OCP-generated lift-mode trajectories within an atmospheric large-eddy-simulation (a high-fidelity induction model), the resulting induction effects are far too large to be safely neglected. Second, [24, 125] find that the inclusion of a quasi-steady actuator model (a very rough induction model) into an OCP leads to a large drop in predicted power. Further, [26] finds that small variations in the specific low-order induction model can cause non-trivial changes to the performance prediction. On this note, [25] suggests that modeling for lift-mode systems may specifically need to include dynamic induction effects.

In summary, offline optimal control is an extremely valuable tool in the prediction of an AWE system's performance, which will become even more useful after the resolution of certain open model-plant mismatch issues.

5.2. Model Predictive Control

Model predictive control (MPC) is an advanced feedback control technique that is particularly useful for constrained multi-input systems, thereby representing a promising candidate for control of AWE systems. While we refer the interested reader to textbooks on MPC such as [111, 126, 127] for a detailed general treatment of MPC, we briefly explain the technique here and report on some applications in AWE system control. MPC uses the online solution of an OCP on a moving horizon of fixed length, which is called the *prediction horizon*. The OCP in MPC has a fixed initial value $\mathbf{x}_0$, which is an estimate of the most current system state, given the available measurement data. The objective and path constraints express our desires regarding the system behaviour, such as tracking of a reference trajectory or satisfaction of operational constraints. Given the fact that an OCP needs to be solved at each sampling time of the MPC control loop, which is computationally expensive, MPC was originally developed in the process

control industry, where high-value processes typically operate at relatively slow time scales (in the range of minutes). With advanced computational power and improved algorithms for embedded optimization, MPC became a viable control technology for significantly faster systems e.g. in robotics, mechatronics, or the automotive industry (with millisecond time scales). As AWE systems typically operate periodically, and can most accurately be described by nonlinear models, the MPC variant most commonly proposed for AWE systems is nonlinear periodic MPC. This method was first investigated in the context of tethered wings in [53, 128, 129] and in the context of pumping mode AWE systems in [104, 130, 131]. Online MPC computations remain one of the challenges for real-world control of AWE systems, but have been investigated in real-time capable and somewhat realistic simulation studies such as [104, 132, 133, 134] for single-kite systems, and [135] for dual-kite systems. Robust MPC of kites was addressed through simulations in [136, 137]. Only a few real-world experiments of MPC control for AWE systems have been realized in proof-of-concept studies on simplified AWE setups [86, 138]. Open-source toolboxes that can be used to generate real-time capable C-code for nonlinear MPC computations include ACADO [139] and acados [140], the latter of which can be accessed with models from the AWE toolbox awebox [124]. The scarcity of real-world MPC applications in the field of AWE is not only attributable to the computational overhead, but also to the modelling and estimation challenges. Nonlinear parameter identification on in-flight data and even experimental design were, however, performed in [141, 142].

5.3. Adaptive Techniques

AWE systems represent complex dynamical systems for which no numerical model is fully accurate, which operate in variable wind environments. Consequently, offline optimizations and even online MPC algorithms alone are not always sufficient for achieving optimal performance. In light of this fact, several adaptive control techniques for online adjustment of flight path parameters and operating altitude have been considered in the literature.

Implementation-wise, one of the simplest mechanisms for online optimization of flight paths and altitudes is extremum seeking (ES), which is described in [143] and consists of the persistent application of a perturbation signal to guide a control parameter to its optimal value. In fact, ES was initially successfully applied to the problem of online altitude optimization for a lighter-than-air AWE system in variable flow in [144]. ES was later used for the optimization of reference parameters that defined a crosswind flight path in [145]. Here, an offline optimization was used to derive a table of optimal Fourier coefficients as a function of wind speed. Because of inevitable model uncertainties, the actual optimal Fourier coefficients would always differ at least slightly from the offline-optimized values. To address this, ES was used to update a "reference wind speed" online, in order to maximize power output.

Because the process of crosswind flight is clearly a repetitive task, with power output following a varying profile over each lap of crosswind flight, tools from repetitive and iterative learning control (ILC) also can be tailored to the optimization of AWE flight paths. Iteration-domain (lap-domain, in this case) tools carry an advantage over time-domain tools in that they can account for the expected variability of the power profile over the course of one cycle. In fact, [89] proposes and validates a lap-domain perturb-and-observe style adaptation law for adjusting the parameters of a figure-8 crosswind flight path. Formal tools from ILC can also be tailored to AWE systems; however, they must be re-tailored to address some unique features of AWE systems that have not been traditionally considered in the ILC literature. In particular, most legacy tools in iterative learning have (i) focused entirely on reference tracking, as opposed to the maximization of some "profitability" metric, (ii) assumed consistent iteration duration (equivalent to consistent lap time for AWE systems), and (iii) assumed (in the case of ILC) a pause between iterations. In order to leverage the general structure of ILC tools while addressing the unique features of AWE systems (and other systems for which the goal is not simply reference tracking, iteration duration is not fixed, and/or there is no pause in operation), Vermillion and his collaborators have developed a new variant on ILC, termed *economic ILC*, described for AWE systems in [61].

The structure of an economic ILC update, when used to adjust the parameters that define a figure-8 flight path, is shown in Figure 21. In the case of crosswind flight, each "iteration" is treated as either (i) one figure-8 or elliptical "lap" (this is done in the case of fly-gen systems in particular, in [61] for example) or (ii) one full reel-out/reel-in cycle, which comprises multiple laps (this is done in the case

of ground-gen systems, in [146] for example). Unlike traditional applications of ILC, where a reference path or trajectory is pre-specified, the path is precisely the quantity to be optimized in the formulation of Figure 21. Specifically, the path, generally following a figure-8 lemniscate, is parameterized in terms of a finite-dimensional *basis vector*, $\mathbf{b}_j$, where j refers to the iteration number. Two updates are performed between each pair of iterations:

1. A response surface, which characterizes performance as a function of the basis parameters, is recursively updated.
2. The basis parameters themselves are updated using a gradient-based or error-based ILC update law.
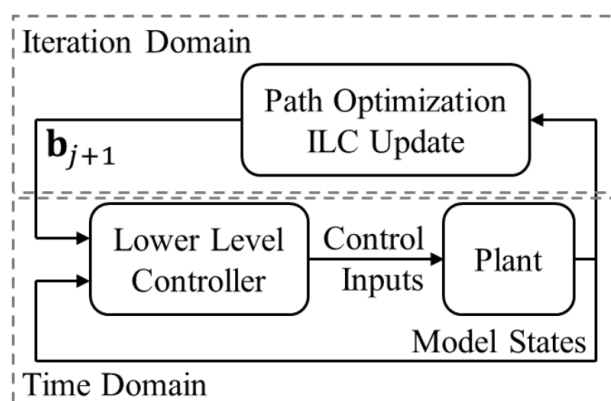

Figure 21: Basic block diagram for economic ILC, as applied to the optimization of the flight path (parameterized through the basis parameters $\mathbf{b_j}$).

The economic ILC formulation was validated for both constant and variable wind profiles in [61]. Figures 22 and 23 show the progression of path geometry and performance as figure-8 laps progress and wind speed is held constant. Performance (to be maximized) is measured by the average power output, in kW, minus a term that penalizes the deviation between the flown and ILC-prescribed course geometry (disincentivizing the generation of paths that cannot be readily tracked). Figures 24-25 turn to variable wind simulations, utilizing openly available wind data obtained from the National Renewable Energy Laboratory (NREL) and shown in Figure 24. Figure 25 illustrates the performance of the economic ILC approach, as compared to a constant-path baseline, under this wind profile. Consideration of both constant and variable wind profiles serve two different and very important purposes. First, the constant wind results make it possible to confirm that the path parameters do indeed converge to their optimal values. The variable wind results confirm that the economic ILC update is fast enough to keep up with the variations in wind speed.

6. Launch and Landing Strategies

Launch and landing phases are critically important for AWE systems. They must be carried out whenever wind conditions are not suitable to generate power, and when the system needs to be landed due, for example, to anomalies and faults. To enable fully autonomous operation of any AWE system for significant time, launch and landing phases must be fully automated, and the supervisory control system must decide when to trigger them. Transitions to and from the power generation phase must also be carried out autonomously. However, in the scientific literature, the contributions related to launch and landing of AWE systems are by far less numerous than those pertaining to crosswind flight control and power generation, both for ground-gen and fly-gen systems. One reason for this gap is that launch and landing phases can be initially carried out by a human pilot, where the system is subsequently switched to autonomous operation. Indeed, launch and landing phases are rather short and carried out at relatively low speeds, so that a pilot can execute them effectively, in contrast with the power generation phase,
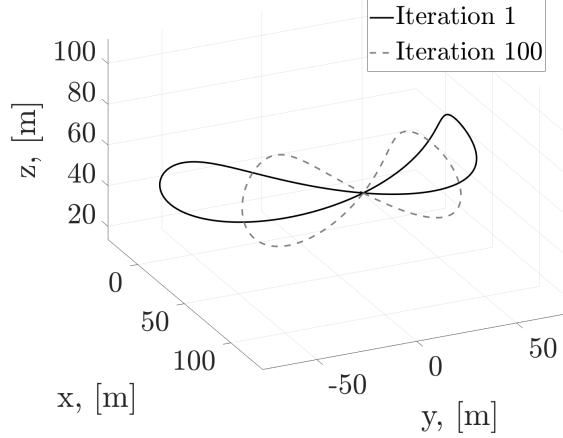
Figure 22: Initial and converged path when using economic ILC under constant wind.

which requires a continuous, high level of attention to obtain good orbit repeatability and stabilize the flight pattern. For small-scale systems employing a soft kite, one business model even assumes that re-positioning of the kite after landing is eventually carried out by a crew, thus having non-fully-autonomous operation (see Figure 26).

As a consequence of the aforementioned factors, the study of the automation problem of launch and landing started several years after that of crosswind flight. For the same reason, the design of systems suitable for fully autonomous, repeatable launch and landing has started in relatively recent times, first for fly-gen systems around 2010, and then for ground-gen systems from around 2014 onward. Today, in the literature, there are studies pertaining to the analysis and comparison of different launch and/or landing options at the system level (see, e.g., [148, 149]), as well as studies on specific solutions and phases [60, 90, 150]. Launch and landing strategies have been also surveyed in the study [151], as this is a key aspect and a possible classification criterion in addition to on-board vs. on-ground generation. While for fly-gen systems a vertical launch and landing strategy is well-established as the most sensible solution, for ground-gen systems there are still several options in the AWE research and development landscape. Currently, the approaches that are pursued by companies and research groups for these systems are the following:

1. *Vertical Take Off and Landing (VTOL)*: Used for rigid kites, this method employs propellers to operate the kite like a multicopter. The system is then automatically guided in hovering mode and transitions to crosswind flight once the operating altitude has been reached. The inverse maneuver is carried out for landing. The concept has also been explored for soft wing kites, by using a multicopter as an additional, but separate lifting device, that is decoupled after launch.

2. *Telescopic mast*: Used for flexible wings, a relatively thin mast is used to lift the kite at a safe height to start a controlled ascent with the leading edge facing the wind. When operational height is reached, the kite is steered into crosswind motion. Landing is carried out through an inverse maneuver. A small tether linking the leading edge to the mast is used to guide the kite in both launch and landing maneuvers. An alternative mast-based launching maneuver is from an upside-down hanging position.

3. *Rotational launch and landing*: A rotating arm is used to accelerate the aircraft to take-off speed, at which point the tether is reeled out at relatively slow speed while rotation continues until a long-enough tether length is reached and the system can transition to power generation. As with the telescopic mast system, an inverse maneuver is carried out for landing. This maneuver has been
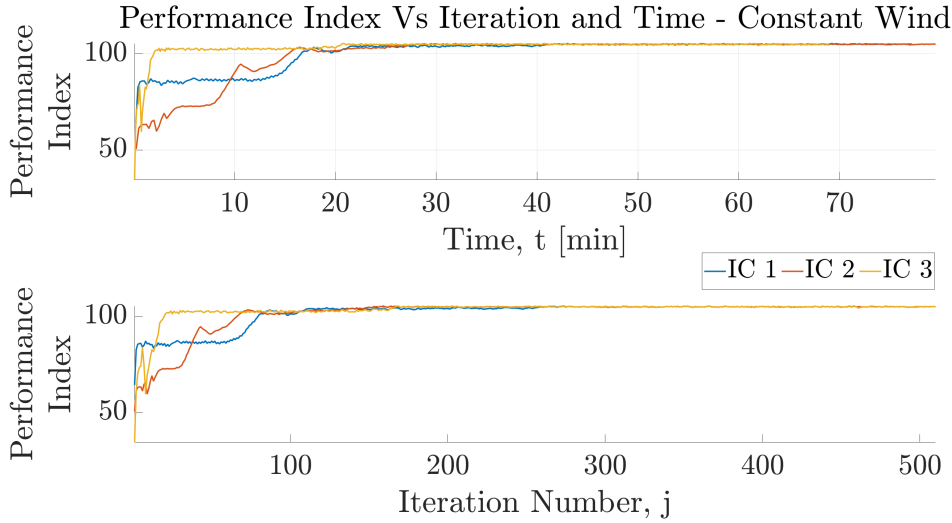
Figure 23: Convergence of performance index to be maximized (Average power, in kW, minus a penalty for the low-level flight controller's deviation from the ILC-defined path) vs. time and iterations (laps), under both ILC and a baseline fixed-path controller.

proposed for both rigid and semi-rigid kites.

4. *Linear launch and landing*: This method is proposed for rigid kites. A linear motion device is used to accelerate the aircraft up to take-off speed, while the tether is reeled out under low traction force. After take-off, the kite climbs to operational height, exploiting suitable on-board propeller(s). The landing phase is similar to that of a conventional airplane: the kite approaches the landing platform sustained by aerodynamic lift, and after touch down is stopped in short distance by means of a suitable braking device.

Besides system-level considerations (see [149]), it is immediately apparent that these launch and landing strategies pose very different control and automation challenges. One sensible way to classify launch and landing approaches from a control viewpoint is based on the speed of the kite relative to ground. Approaches 1 and 2 involve relatively low speeds, while approaches 3 and 4 involve much larger speeds. One challenge of low-speed maneuvers is that the effect of wind turbulence is relatively stronger as compared to the available control authority, and increasing control authority generally implies increasing the system mass, which is not desirable for the sake of power generation performance. On the other hand, an advantage of low-speed approaches is that there is more time to react if something does not work as planned. Given that launch and landing maneuvers are carried out partly very close to ground, this aspect is crucial from a safety standpoint. On the contrary, high-speed maneuvers benefit from higher control authority thanks to large apparent speeds, but the involved risk when maneuvering close to ground is larger as well. Specific feedback control strategies for launch and/or landing phases are presented in [90] (linear take-off), [150] (vertical take-off and landing for flexible kites), and [60] (vertical take-off and landing for rigid kites).

It is important to remark that launch and landing maneuvers are supposed to take negligible overall time in the lifetime of an AWE system as compared with power generation and on-ground storage. However, the *number* of launch and landing events can be very large, and every such event can imply a rather high risk for the system integrity when maneuvering close to ground, especially at high speed. As an example, consider an AWE system farm with 20 units. Assuming on average 1/2 launch and landing events per day every year (which can be rather optimistic, considering that the system needs to land whenever the wind speed is not large enough to keep the aircraft and tether airborne without consuming energy), in 10 years of operation the AWE farm will experience in total 36500 launch and
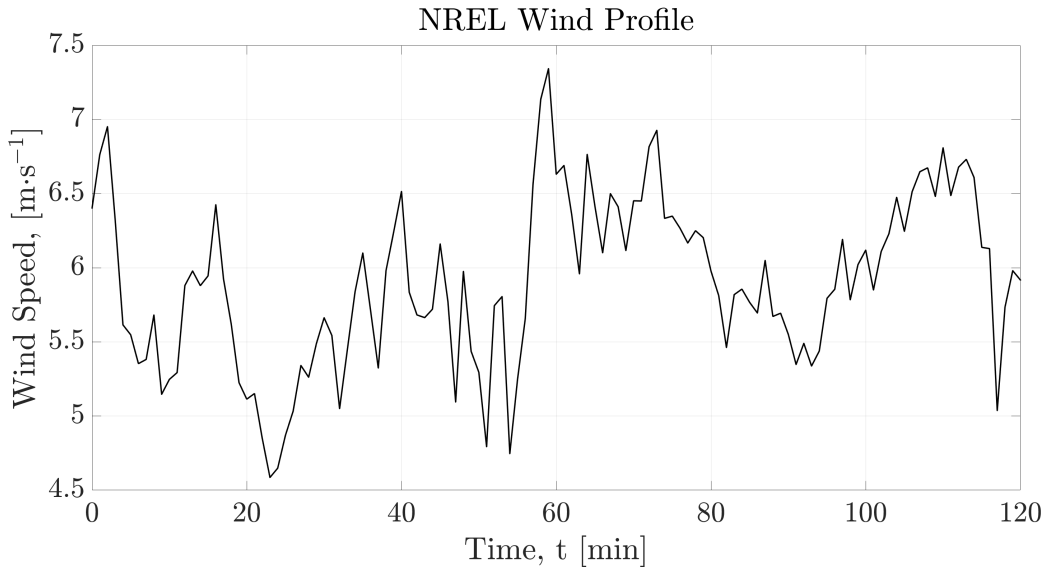
Figure 24: Wind profile, as obtained from NREL, used for validation of the economic ILC strategy in variable wind environments.

landing maneuvers. One critical parameter that affects the capability to operate at lower wind speed (hence reducing the number of launch and landing events) is the specific mass of the aircraft, i.e. its mass divided by its reference area. The same quantity also affects the energy required to launch the system [149].

Due to their critical, enabling role for large-scale implementation of AWE systems and the current relatively scarce scientific literature pertaining to their design and control, launch and landing phases are one of the most important and pressing topics for further research and development in AWE systems.

7. Experimental Results

One of the greatest developments in the AWE community over the last fifteen years has been the move from paper to practice, with dozens of research labs, multi-institution consortia, and companies deploying prototypes at a variety of scales. The prototypes have run the gamut from lab-scale demonstrations to prototypes for field tests with increasing functionality and scale.

7.1. Lab-scale testing frameworks

A number of university teams have developed lab-scale, indoor frameworks for validating attributes of tethered systems. These have allowed for rapid prototyping of new designs and controllers at cost levels that were manageable on typical project budgets.

One of the most well-known lab-scale experimental platforms is the water channel-based platform developed at the North Carolina State University. In this testing framework, depicted in Figure 27, 3D printed models are tethered and flown under closed-loop control in a water channel. The use of the water channel, rather than a wind tunnel, enables achievement of dynamic similarity with regard to all dimensionless variables except for Reynolds number, which still exhibits a significant difference between the two scales (see [152, 153]). Under scenarios where fluid dynamic coefficients remain consistent between the two testing environments, dynamic similarity under open- and closed-loop flight has in fact been confirmed in [152, 153]. In other scenarios, where exact dynamic similarity is unachievable, the water channel framework provides a mechanism for refining and validating a dynamic model, which can subsequently be extrapolated to full-scale flight. The latter has in fact been performed recently, with comparisons of experimental results and model predictions shown in Figure 28 and further details provided in [154].
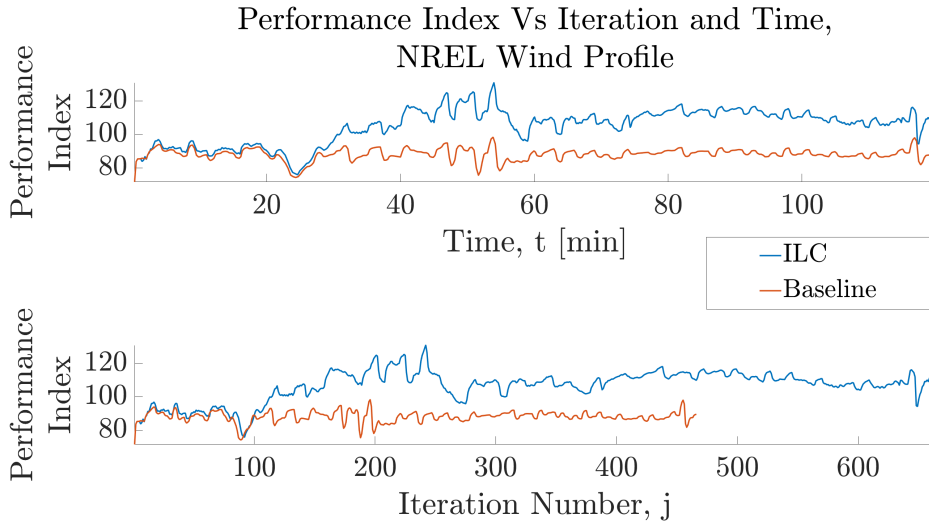
Figure 25: Performance index (average power output (kW) minus tracking penalty) under the economic ILC approach - Initial condition (IC) 1.

Another example of a small-scale setup is the indoor carousel developed at KU Leuven and at the University of Freiburg, described in [155]. This setup is designed to study the rotational take-off and landing of rigid kites, focusing in particular on the sensor fusion and automatic control aspects of these phases. Interestingly, such small-scale setups also allow researchers to investigate and test technologies that are enabling for airborne wind, yet have a broader scope and impact on their own, as is the case of the embedded optimization and automatic code generation for model predictive control application described in [155].

7.2. Prototypes for field tests

One initial barrier to research and development in AWE, which led to the development of small-scale setups described above, stems from a fundamental feature of AWE systems: given that AWE systems remain airborne by executing rather large flight patterns in a prevailing wind resource, one needs to find a good, windy site and a large enough testing space free from obstacles. It is not surprising then that most prototypes built for field tests are movable, installed either on a truck or on a trailer. Tow-test experiments, where a ground station is moved to artificially generate a controllable wind flow, have become a popular immediate method for testing AWE systems [86, 156]. Testing of a stationary system in a relatively remote site, away from offices and labs, immediately increases cost, time and complexity of test procedures and thus requires some time and accumulated experience before proving effective. This is another feature of AWE research: there is a rather abrupt step from lab-scale systems to field tests, and little compromise in between.

In the literature, there are many examples of prototypes for field tests, making a detailed description of each impossible within the space of a single survey paper. These prototypes are visible in many videos available on the web, as well in papers, book chapters, and books of abstracts [28, 51, 52, 90, 92, 157, 158]. For most of these systems, their design, operation, and performance are not fully described and readily available from the literature, having been built and operated by companies and subject to confidentiality. On the other hand, some of these prototypes for field tests have been explicitly conceived and built by research institutions with the goal of advancing fundamental AWE research and disseminating the resulting knowledge as much as possible – see Figure 29 for examples. This is the case, for example, of the small-scale prototype built at UC Santa Barbara with funding from both E.U. and U.S. bodies and in a collaborative effort among UCSB, ETH Zurich, and Politecnico di Torino, employed to investigate crosswind

29

Figure 26: Experimental launch of a 25 m^2 V3 leading edge inflatable tube kite from an upside-down hanging position on 23 August 2012 (top), standard half-automated winch launch of a 40 m^2 V5.40 derivate kite, temporarily reaching a tether force of 15 kN and a mechanical power of 100 kW during a test flight in May 2018 (bottom) [147].

flight and kite steering dynamics [51], as well as the prototype developed by ABB Corporate Research to investigate autonomous linear take-off [90, 160], the one developed within the Swiss Kite Power Initiative among ETH Zurich, FHNW Schweiz, and EMPA, able to carry out full power cycles [55], and the one developed at UF Santa Catarina [92]. For some of these systems, rather detailed descriptions of their main design guidelines are present in the literature as well [159, 160], available for other researchers as a starting base to further improve and push forward the research frontier.

An extensive research data set for a pumping kite power system using a flexible membrane wing with suspended kite control unit was created by Delft University of Technology [41, 161]. Originally intended as validation data for performance models, this data was extended through a detailed aerodynamic characterization of a 25 m^2 leading edge inflatable tube kite with suspended kite control unit [162] and supplemented by an open access data set [163]. A 6 m^2 soft kite system with a suspended kite control unit was used for towing tests by Kyushu University, to explore the potential of machine learning [164]. The data set is available in open access form [156, 165].

Finally, as an example of a publicly available data set for a large-scale rigid AWE system, Makani Power recently released an extensive set of source code [42], test logs [43], and technical videos [44].
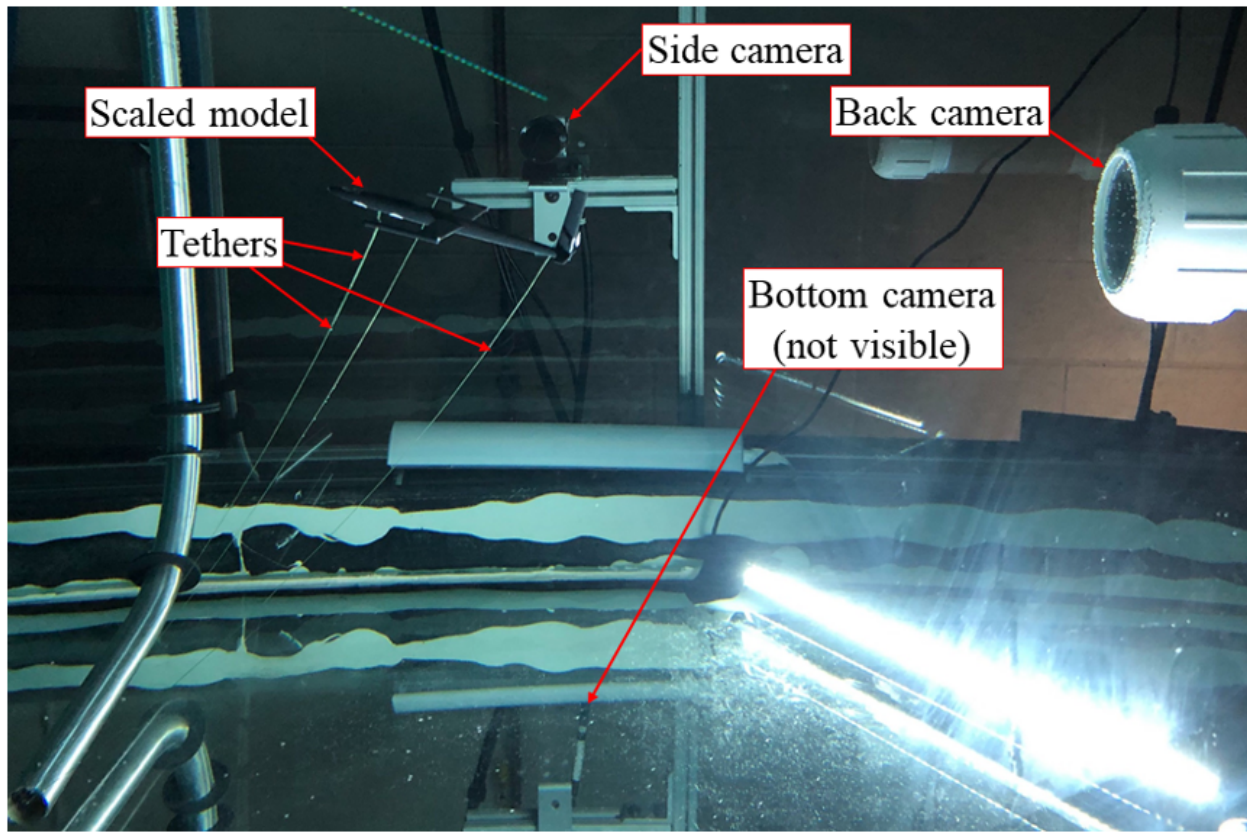
Figure 27: Water channel-based lap-scale setup for closed-loop characterization of tethered systems.

This release followed the unfortunate discontinuation of the company but represents a vast open-source knowledge base for the entirety of the AWE community. These reports comprise 13 years of technical development and provide complete modeling and control source code and corresponding test results for the Makani M600.

8. Other Applications of AWE Technology

In this section, we examine the power-generation potential and early results related to an extension of AWE systems for a highly promising sister application, namely underwater energy harvesting. Specifically, tethered underwater kites that extract energy from ocean currents, tidal flows or rivers are examined. Here, researchers have begun to leverage the principles of operation for AWE systems, including cross-*current* flight, to develop a new type of underwater energy generator.

Figure 30 shows ocean kite system concepts (sometimes referred to as tethered undersea kites, or TUSKs) with major components similar to AWE systems. Ocean kites use rigid wings, fuselages and control surfaces, since weight is less of a consideration and flexible kites are much more difficult to manage underwater. The power generator can be located either on the kite, or on the seabed. Some proposed configurations also locate the generator near the ocean surface on a floating-moored platform (in deep-water currents) or a fixed-monopile platform (in shallow currents). On-board turbines or a standard pumping cycle of high-tension reel-out under cross-current flight, followed by low-tension reel-in, are used as in AWE systems.

Substantial power output increases for ocean kites compared to fixed marine turbines have been estimated and verified [166, 168]. Another advantage of ocean kites is that power densities in typical marine

flows are generally six to seven times higher than in wind flows, assuming marine and wind velocities of 1 m/s and 5 m/s, respectively. Ocean kites can also have small cosine losses [169], particularly for surface-mounted generators. This is because the higher current velocities, which occur near the ocean surface, can be accessed with a smaller tether angle [168]. Seabed-mounted generators in shallow water can also achieve low cosine losses. Finally, issues with kite launch and control during slack current conditions are reduced for neutrally buoyant ocean kites.

Tethered ocean systems, however, must withstand the challenging marine environment. Materials, especially for underwater wings and tethers, need to be carefully selected. Floating or fixed platform foundations need to be properly designed to withstand tether, current and wave loading. The effect on marine animals and shipping operations also needs further study.

Kites for marine hydrokinetic energy generation were first proposed by Landberg [170]. Along with a conceptual ocean kite diagram, Figure 30 shows ocean kites from Minesto, Ltd. and SeaQurrent. Minesto's Deep Green technology, with a kite-mounted turbine and generator, has been developed at commercial scale, with a 500 kW device off the coast of Wales that has validated procedures for offshore operations. SeaQurrent, which employs a two-kite pumping cycle with a power take-off generator fixed to the seabed, has deployed a 1:10 scale-model TidalKite in the North Sea. Taking advantage of the fact that windy coastal areas often also have fast currents, a hybrid scheme was recently studied that combines AWE and ocean kites deployed off a single floating platform [171].

An extensive literature search on ocean kites, including the recent hydrokinetic energy reviews [172, 173, 174], reveals only a handful publications. An economic analysis on Minesto's Deep Green technology for the Agulas Current near South Africa calculated weight/power ratios of 14, 50-600, and 200 Tonnes/MW for Deep Green, conventional marine hydrokinetic (MHK) turbines, and shallow water offshore wind turbines, respectively [175]. A levelized cost of energy analysis yielded US $0.081 - 0.19$/kWh for Deep Green, US $0.20 - 0.41$/kWh for MHK turbines, and US $0.13 - 0.16$/kWh for offshore wind turbines.

In an early study, Olinger and Wang [168] estimated maximum theoretical power output for ocean kites and made detailed comparisons of key performance parameters with conventional marine turbines. Some preliminary design considerations for the kite, floating platforms, tether, turbines and control surfaces were considered. Governing equations of motion to study the dynamics of the kite were developed, and a baseline simulation that used a simple proportional kite attitude control scheme estimated kite trajectories, kite pitch, roll and yaw dynamics, power output, kite hydrodynamic forces, and tether tensions. The potential for cavitation on turbine blade tips was also studied.

A computational simulation for an ocean kite in two-dimensional motion used a regular structured grid to resolve the ocean current flow, and domain-immersed boundary methods and open multiprocessing (OpenMP) were employed to solve the Navier-Stokes flow equations [176]. The reel-out and reel-in velocities of the two tethers were adjusted to control the kite angle of attack and the resultant hydrodynamic forces. A baseline simulation yielded net power output during successive kite power and retraction cycles, and vorticity flow fields, tether tensions, and kite hydrodynamic coefficients were determined. The power output results were shown to be in good agreement with Loyd [37] for a kite moving in two dimensions. A 6-dof rigid kite and beaded tether (KMBT) model describes the trajectory and attitude of an underwater kite [177]. The attitude movement stability of the kite body under the action of the tether tension and the influence of kite bridle length on the motion stability were analyzed. Results from an underwater kite experiment were compared to both KMBT simulation results and a simpler kite-without-tether model. The results showed that KMBT can describe the motion of the kite more accurately.

These computational simulations were extended to model the cross-current flight of a full-scale ocean kite by adding a moving computational grid [178]. The kite pitch, roll and yaw angles during power and retraction phases were adjusted using a PID control method to achieve the desired cross-current kite trajectories. The effect of tether drag on the resulting power output was also investigated. Predictions from these simulations [179] were shown to be in good agreement with Luchsinger [40] for optimum power output, tether reel-out to reel-in speeds, tether force ratios, and reel-in to reel-out power ratios. The dynamics and control of ocean kites has been studied in [180] by applying a 6-dof, rigid-body model that includes hydrodynamic, added mass, gravity and buoyancy force effects. The stability of the kite

and the passivity property of the hydrodynamic force were investigated. An input-output system, based on the kite dynamics and a passivity-based control algorithm were designed. A baseline simulation was used to verify successive cyclic power generation under the proposed control scheme.

As with AWE systems, successful demonstration of cross-current flight under tracking controllers gave way to a (relatively small to-date) body of research on the optimal control of ocean kite systems. Paiva and Fontes [181] developed a dynamical continuous-time model and optimal control formulation for an underwater power kite and obtained the trajectories and controls that maximize the total energy produced in a given time interval. A numerical solution scheme for the optimal control problem based on direct methods and on adaptive time-mesh refinement was also developed. The numerical scheme provided a set of output power values for different design choices and confirmed that net electrical energy can be produced. A complementary effort by Daniels et. al. [182] presents a continuous-time optimal control formulation for spooling control. This effort utilizes a detailed dynamic model to derive a lower-order metamodel, which is in turn used, in conjunction with Pontryagin's Maximum Principle, to optimize the spooling speed trajectory. Selected results were shown for an ocean kite system, demonstrating up to a 45 percent increase in average net power output as compared with a baseline strategy. It is worth noting that the optimal control strategy detailed in [182] can also be applied to airborne systems. The authors of [146] present an application of aforementioned ILC strategies for the optimization of path geometries for an ocean kite system. Finally, a mathematical model of an ocean kite's power generation system using maximum-power-point-tracking (MPPT) algorithms and closed-loop speed controllers has been developed [183]. Experimental results on a 35-kVA laboratory emulator are presented, and an accurate representation of the system dynamics and inertia are implemented.

Further studies on ocean kites are needed to realize the full potential of this nascent technology. Modeling, simulations, and control systems for AWE systems that have been summarized in earlier sections of this review can be further applied to ocean kites after relevant physics, including added mass and buoyancy effects, are included. For example, some studies [146] have recently incorporated a general modeling framework for tethered energy systems applicable to AWE or ocean kites. This has been expanded into a highly general modeling framework that considers both the kite and 4D (x, y, z, and time) spatiotemporally varying flow environment, which is detailed in [184]. Selected flight simulation results are shown in Figure 31.

9. Conclusions

Airborne wind energy (AWE) represents a promising technology that has grown over the past decade from a tight cluster of organizations pursuing initial concept designs to a thriving research and development field consisting of over 60 institutions worldwide. Just as the size of the AWE community has grown over the past decade, so has the maturity of both the control architectures used to harvest the wind energy and the prototypes – both small and large – that have been used to demonstrate the efficacy of AWE systems. In particular, and as demonstrated in this work, control approaches have matured from simple strategies aimed at robustly tracking crosswind patterns under mild conditions, to optimal control strategies for maximizing wind power in varying environmental conditions and modal control approaches for robustly launching and landing AWE systems. Prototypes have gone from small demonstrators using fabric kites to 600 kW+ power-producing prototypes. Given this record of progress, as documented in this survey paper, a bright future exists for the field.
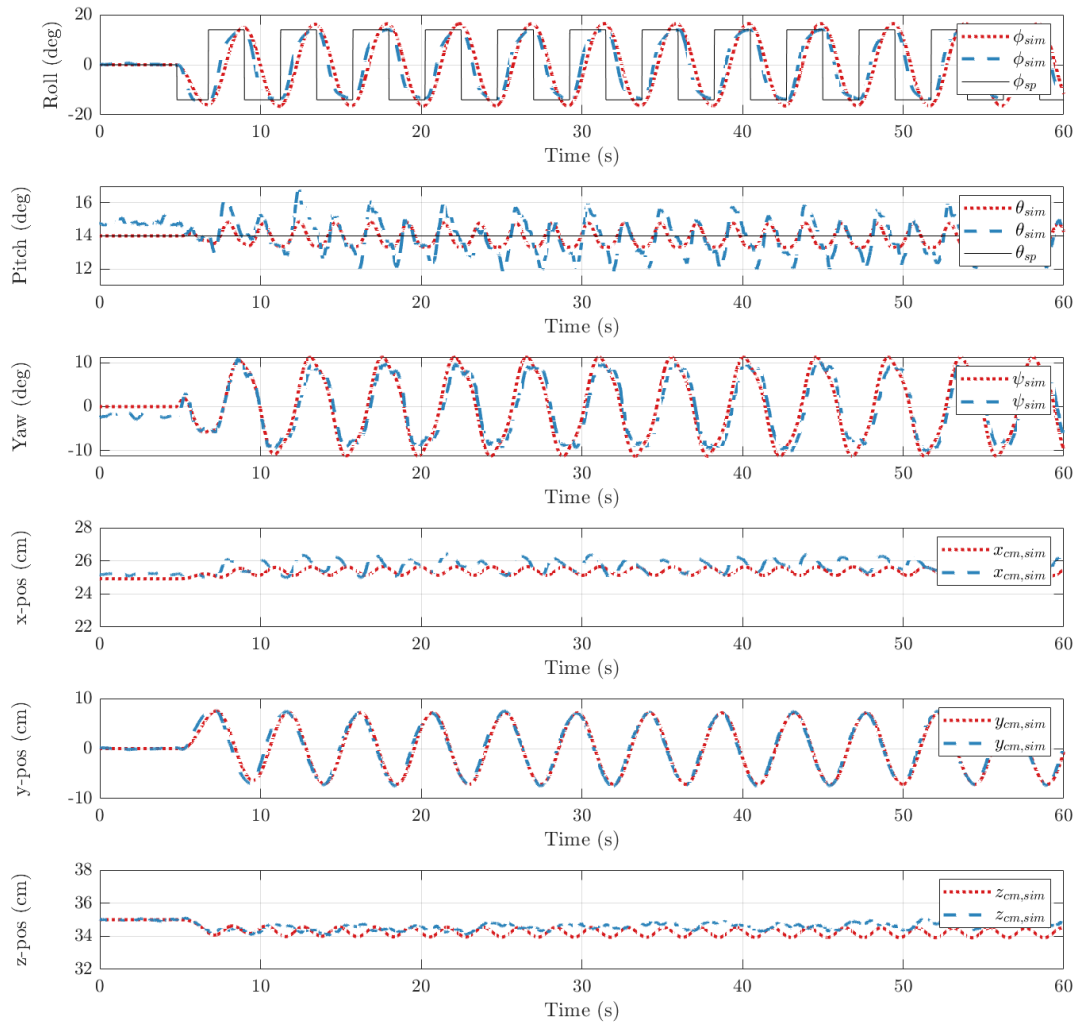
Figure 28: Comparison of dynamic model predictions and experiments for a lab-scale tethered energy system.

Figure 29: Examples of prototypes for field tests whose results and data are available to the research and development community. Clockwise from top left: UCSB prototype [51, 159], Swiss Kite Power prototype [55], ABB Corp. Res. prototype [160, 90].

Figure 30: Major components of an ocean kite system [146]; Minesto Deep Green [166]; and SeaQurrent Tidal Kite [167].
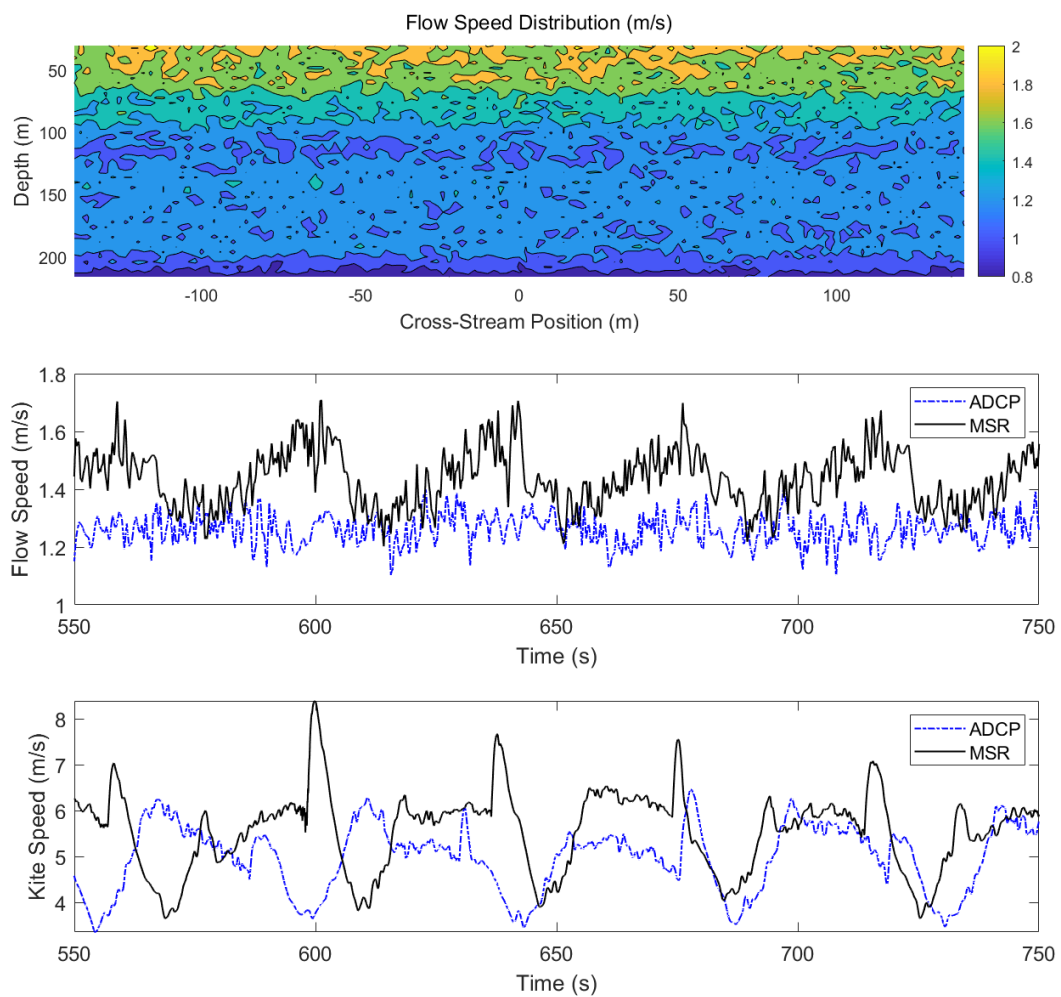

Figure 31: Simulated ocean kite performance in a spatiotemporally varying ocean environment, including a snapshot of the 2D flow field perpendicular to the current (left), local flow speed at the kite vs. time (middle), and kite speed vs. time (right).

References

[1] Wind technologies market report, U.S. Department of Energy (2018).

[2] P. Jamieson, Innovation in Wind Turbine Design, 2nd Edition, John Wiley & Sons, Hoboken, NJ, 2018.

[3] V. Nelson, Innovative Wind Turbines: An Illustrated Guidebook, CRC Press, Boca Raton, FL, 2019. doi:10.1201/9781003010883.

[4] S. Watson, A. Moro, et al., Future emerging technologies in the wind power sector: A European perspective, Renewable and Sustainable Energy Reviews 113 (2019) 109270. doi:10.1016/j.rser.2019.109270.

[5] G. Abbate, E. Saraceno, What else is emerging from the horizon?, in: A. Vasel, D. S.-K. Ting (Eds.), Advances in Sustainable Energy, Springer International Publishing, Cham, 2019, pp. 177–213. doi:10.1007/978-3-030-05636-0_10.

[6] M. Erhard, H. Strauch, Automatic control of pumping cycles for the skysails prototype in airborne wind energy, in: R. Schmehl (Ed.), Airborne Wind Energy – Advances in Technology Development and Research, Green Energy and Technology, Springer, Singapore, 2018, Ch. 9, pp. 189–213. doi:10.1007/978-981-10-1947-0_9.

[7] B. MacCleery, The advent of airborne wind power, Wind Systems Magazine (1) (1 2011).
URL https://www.windsystemsmag.com/the-advent-of-airborne-wind-power

[8] A. Bormann, M. Ranneberg, P. Kövesdi, C. Gebhardt, S. Skutnik, Development of a three-line ground-actuated airborne wind energy converter, in: U. Ahrens, M. Diehl, R. Schmehl (Eds.), Airborne Wind Energy, Green Energy and Technology, Springer, Berlin Heidelberg, 2013, Ch. 24, pp. 427–437. doi:10.1007/978-3-642-39965-7_24.

[9] V. Salma, F. Friedl, R. Schmehl, Improving reliability and safety of airborne wind energy systems, Wind Energy 23 (2) (2019) 340–356. doi:10.1002/we.2433.

[10] M. Aull, K. Cohen, A nonlinear inverse model for airborne wind energy system analysis, control, and design optimization, Wind Energy (2020). doi:10.1002/we.2562.

[11] A. Candade, M. Ranneberg, R. Schmehl, Structural analysis and optimization of a tethered swept wing for airborne wind energy generation, Wind Energy 23 (4) (2020) 1006–1025. doi:10.1002/we.2469.

[12] J. Wijnja, R. Schmehl, R. De Breuker, K. Jensen, D. Vander Lind, Aero-elastic analysis of a large airborne wind turbine, Journal of Guidance, Control and Dynamics 41 (11) (2018) 2374–2385. doi:10.2514/1.G001663.

[13] F. Bauer, D. Petzold, R. M. Kennel, F. Campagnolo, R. Schmehl, Control of a drag power kite over the entire wind speed range, Journal of Guidance, Control, and Dynamics 42 (10) (2019) 2167–2182. doi:10.2514/1.G004207.

[14] B. Ahrens, Uwe amd Pieper, C. Töpfer, Combining kites and rail technology into a traction-based airborne wind energy plant, in: U. Ahrens, M. Diehl, R. Schmehl (Eds.), Airborne Wind Energy, Green Energy and Technology, Springer, Berlin Heidelberg, 2013, Ch. 25, pp. 437–441. doi:10.1007/978-3-642-39965-7_25.

[15] B. W. Roberts, Quad-rotorcraft to harness high-altitude wind energy, in: R. Schmehl (Ed.), Airborne Wind Energy – Advances in Technology Development and Research, Green Energy and Technology, Springer, Singapore, 2018, Ch. 23, pp. 581–601. doi:10.1007/978-981-10-1947-0_23.

[16] P. Benhaïem, R. Schmehl, Airborne wind energy conversion using a rotating reel system, in: R. Schmehl (Ed.), Airborne Wind Energy – Advances in Technology Development and Research, Green Energy and Technology, Springer, Singapore, 2018, Ch. 22, pp. 539–577. doi:10.1007/978-981-10-1947-0_22.

[17] C. Beaupoil, Practical experiences with a torsion based rigid blade rotary airborne wind energy system with ground based power generation, in: R. Schmehl, O. Tulloch (Eds.), Book of Abstracts of the International Airborne Wind Energy Conference 2019, University of Strathclyde, Glasgow, United Kingdom, 2019, pp. 146–147.
URL http://resolver.tudelft.nl/uuid:c50f7eb6-f116-4158-9e9b-aa1b05092ab2

[18] O. Tulloch, A. Kazemi Amiri, H. Yue, J. Feuchtwang, R. Read, Tensile rotary power transmission model development for airborne wind energy systems, Journal of Physics: Conference Series 1618 (2020) 032001. doi:10.1088/1742-6596/1618/3/032001.

[19] M. Garia-Sanz, N. White, N. Tierno, A Novel Approach to Airborne Wind Energy: Overview of the EAGLE System Project, in: Proceedings of the IEEE National Aerospace & Electronics Conference, Dayton, Ohio, 2011, pp. 167–172. doi:10.1109/NAECON.2011.6183096.

[20] C. Vermillion, B. Glass, A. Rein, Lighter-than-air wind energy systems, in: U. Ahrens, M. Diehl, R. Schmehl (Eds.), Airborne Wind Energy, Green Energy and Technology, Springer, Berlin Heidelberg, 2013, Ch. 30, pp. 501–514. doi:10.1007/978-3-642-39965-7_30.

[21] R. J. Penedo, T. C. Pardal, P. M. Silva, N. M. Fernandes, T. R. C. Fernandes, High altitudewind energy from a hybrid lighter-than-air platform using the magnus effect, in: U. Ahrens, M. Diehl, R. Schmehl (Eds.), Airborne Wind Energy, Green Energy and Technology, Springer, Berlin Heidelberg, 2013, Ch. 29, pp. 491–500. doi:10.1007/978-3-642-39965-7_29.

[22] T. Bronnenmeyer, Optimal Control for Multi-Kite Emergency Trajectories (MSc thesis), University of Stuttgart, Stuttgart, Germany, 2018.

[23] J. De Schutter, R. Leuthold, M. Diehl, Optimal Control of a Rigid-Wing Rotary Kite System for Airborne Wind Energy, in: Proceedings of the European Control Conference (ECC), Limassol, Cyprus, 2018, pp. 1734–1739. doi:10.23919/ECC.2018.8550383.

[24] R. Leuthold, S. Gros, M. Diehl, Induction in optimal control of multiple-kite airborne wind energy systems, IFAC-PapersOnLine 50 (1) (2017) 153–158, 20th IFAC World Congress. doi:10.1016/j.ifacol.2017.08.026.

[25] R. Leuthold, J. De Schutter, E. Malz, G. Licitra, S. Gros, M. Diehl, Operational Regions of a Multi-Kite AWE System, in: Proceedings of the European Control Conference (ECC), Limassol, Cyprus, 2018, pp. 52–57. doi:10.23919/ECC.2018.8550199.

[26] R. Leuthold, J. De Schutter, T. Bronnenmeyer, S. Gros, M. Diehl, Comparison of Engineering Induction Models in a Multi-Kite Optimal Control Problem, in: Book of Abstracts of the International Airborne Wind Energy Conference 2019, University of

Strathclyde, Glasgow, United Kingdom, 2019.
URL http://resolver.tudelft.nl/uuid:be84d15b-e7cd-40b4-9561-980f0cf11432

[27] M. Canale, L. Fagiano, M. Milanese, M. Ippolito, Kitegen project: Control as key technology for a quantum leap in wind energy generators, in: Proceedings of the American Control Conference, New York, NY, 2007, pp. 3522–3528. doi:10.1109/ACC.2007.4282697.

[28] R. Schmehl, O. Tulloch (Eds.), Book of Abstracts of the International Airborne Wind Energy Conference 2019, University of Strathclyde, Glasgow, United Kingdom, 2019. doi:10.4233/uuid:57fd203c-e069-11e9-9fcb-441ea15f7c9c.

[29] R. Schmehl, Airborne wind energy – an introduction to an emerging technology, accessed 30 June 2020.
URL http://www.awesco.eu/awe-explained/

[30] C. Archer, K. Caldeira, Global assessment of high-altitude wind power, Energies 2 (2) (2009) 307–319. doi:10.3390/en20200307.

[31] P. Bechtle, M. Schelbergen, R. Schmehl, U. Zillmann, S. Watson, Airborne wind energy resource analysis, Renewable Energy 141 (2019) 1103–1116. doi:10.1016/j.renene.2019.03.118.

[32] M. Schelbergen, P. C. Kalverla, R. Schmehl, S. J. Watson, Clustering wind profile shapes to estimate airborne wind energy production, Wind Energy Science 5 (3) (2020) 1097–1120. doi:10.5194/wes-5-1097-2020.

[33] A. Bafandeh, C. Vermillion, Altitude optimization of airborne wind energy systems via switched extremum seeking - design, analysis, and economic assessment, IEEE Transactions on Control Systems Technology 25 (6) (2016) 2022–2033. doi:10.1109/TCST.2016.2632534.

[34] A. Baheri, S. Bin-Karim, A. Bafandeh, C. Vermillion, Real-time control using Bayesian optimization: A case study in airborne wind energy systems, Control Engineering Practice 69 (2017) 131–140. doi:10.1016/j.conengprac.2017.09.007.

[35] R. H. Luchsinger, et al., Twingtec's roadmap from full proof of concept to the first commercial product, in: R. Schmehl, O. Tulloch (Eds.), Book of Abstracts of the International Airborne Wind Energy Conference 2019, University of Strathclyde, Glasgow, United Kingdom, 2019, pp. 103–107.
URL http://resolver.tudelft.nl/uuid:c5838af6-a0dd-4beb-b5e7-6c97ef74bd0a

[36] M. Kruijff, R. Ruiterkamp, A roadmap towards airborne wind energy in the utility sector, in: R. Schmehl (Ed.), Airborne Wind Energy – Advances in Technology Development and Research, Green Energy and Technology, Springer, Singapore, 2018, Ch. 26, pp. 643–662. doi:10.1007/978-981-10-1947-0_26.

[37] M. L. Loyd, Crosswind kite power, Journal of Energy 4 (3) (1980) 106–111. doi:10.2514/3.48021.

[38] I. Argatov, P. Rautakorpi, R. Silvennoinen, Estimation of the mechanical energy output of the kite wind generator, Renewable Energy 34 (6) (2009) 1525–1532. doi:10.1016/j.renene.2008.11.001.

[39] R. Schmehl, M. Noom, R. van der Vlugt, Traction power generation with tethered wings, in: U. Ahrens, M. Diehl, R. Schmehl (Eds.), Airborne Wind Energy, Green Energy and Technology, Springer, Berlin Heidelberg, 2013, Ch. 2, pp. 23–45. doi:10.1007/978-3-642-39965-7_2.

[40] R. H. Luchsinger, Pumping cycle kite power, in: U. Ahrens, M. Diehl, R. Schmehl (Eds.), Airborne Wind Energy, Green Energy and Technology, Springer, Berlin Heidelberg, 2013, Ch. 3, pp. 47–64. doi:10.1007/978-3-642-39965-7_3.

[41] R. van der Vlugt, A. Bley, R. Schmehl, M. Noom, Quasi-steady model of a pumping kite power system, Renewable Energy 131 (2019) 83–99. doi:10.1016/j.renene.2018.07.023.

[42] Makani open-source code (2020).
URL https://github.com/google/makani

[43] Makani Flight Logs (2020).
URL https://console.cloud.google.com/marketplace/product/bigquery-public-datasets/makani-logs

[44] Makani Technical Videos (2020).
URL https://archive.org/details/makani-power

[45] B. Houska, M. Diehl, Optimal control for power generating kites, in: Proceedings of the European Control Conference (ECC), Kos, Greece, 2007, pp. 3560–3567.

[46] A. Betz, Windenergie und ihre Ausnutzung durch Windmühlen, Vandenhoeck, Göttingen, 1926.

[47] M. Zanon, S. Gros, J. Andersson, M. Diehl, Airborne wind energy based on dual airfoils, IEEE Transactions on Control Systems Technology 21 (4) (2013) 1215–1222. doi:10.1109/TCST.2013.2257781.

[48] J. De Schutter, R. Leuthold, T. Bronnenmeyer, R. Paelinck, M. Diehl, Optimal control of stacked multi-kite systems for utility-scale airborne wind energy, in: Proceedings of the 2019 IEEE 58th Conference on Decision and Control (CDC), 2019, pp. 4865–4870. doi:10.1109/CDC40024.2019.9030026.

[49] T. Haas, J. De Schutter, M. Diehl, J. Meyers, Wake characteristics of pumping mode airborne wind energy systems, Journal of Physics: Conference Series 1256 (012016) (2019). doi:10.1088/1742-6596/1256/1/012016.

[50] F. Trevisi, M. Gaunaa, M. McWilliam, Unified engineering models for the performance and cost of ground-gen and fly-gen crosswind airborne wind energy systems, Renewable Energy (2020). doi:10.1016/j.renene.2020.07.129.

[51] L. Fagiano, A. Zgraggen, M. Morari, M. Khammash, Automatic crosswind flight of tethered wings for airborne wind energy: modeling, control design and experimental results, IEEE Transactions on Control Systems Technology 22 (4) (2014) 1433–1447. doi:10.1109/TCST.2013.2279592.

[52] M. Erhard, H. Strauch, Flight control of tethered kites in autonomous pumping cycles for airborne wind energy, Control Engineering Practice 40 (2015) 13–26. doi:10.1016/j.conengprac.2015.03.001.

[53] M. Diehl, L. Magni, G. D. Nicolao, Efficient NMPC of unstable periodic systems using approximate infinite horizon closed loop costing, Annual Reviews in Control 28 (1) (2004) 37–45. doi:10.1016/j.arcontrol.2004.01.011.

[54] T. A. Wood, H. Hesse, M. Polzin, E. Ahbe, R. S. Smith, Modeling, identification, estimation and adaptation for the control of power-generating kites, Proc. of the 18th IFAC Symposium on System Identification 51 (2018) 981–989. doi:10.1016/j.ifacol.2018.09.066.

[55] A. U. Zgraggen, L. Fagiano, M. Morari, Automatic retraction and full-cycle operation for a class of airborne wind energy generators, IEEE Transactions on Control Systems Technology 24 (2) (2016) 594–698. doi:10.1109/TCST.2015.2452230.

[56] T. A. Wood, H. Hesse, A. U. Zgraggen, R. S. Smith, Model-based identification and control of the velocity vector orientation for autonomous kites, in: 2015 American Control Conference (ACC), IEEE, 2015, pp. 2377–2382.

[57] A. Roullier, Experimental analysis of a kite system's dynamics, Master's thesis, EPFL (March 2020).

[58] M. Erhard, H. Strauch, Control of towing kites for seagoing vessels, IEEE Transactions on Control Systems Technology 21 (5) (2013) 1629–1640. doi:10.1109/TCST.2012.2221093.

[59] T. A. Wood, H. Hesse, A. U. Zgraggen, R. S. Smith, Model-based path planning and tracking for tethered wings, Proc. of the IEEE Conference on Decision and Control 54 (2015). doi:10.1109/CDC.2015.7403276.

[60] D. Todeschini, L. Fagiano, C. Micheli, A. Cattano, Control of a rigid wing pumping airborne wind energy system in all operational phases, Control Engineering Practice (2020). arXiv:2006.11141.
URL https://arxiv.org/abs/2006.11141

[61] M. Cobb, K. Barton, H. Fathy, C. Vermillion, Iterative learning-based path optimization for repetitive path planning, with application to 3-d crosswind flight of airborne wind energy systems, IEEE Transactions on Control Systems Technology 28 (4) (2019) 1447–1459. doi:10.1109/TCST.2019.2912345.

[62] P. Nikpoorparizi, N. Deodhar, C. Vermillion, Modeling, control design, and combined plant/controller optimization for an energy-harvesting tethered wing, IEEE Transactions on Control Systems Technology 26 (4) (2018) 1157–1169. doi:10.1109/TCST.2019.2721361.

[63] C. Vermillion, T. Grunnagle, R. Lim, I. Kolmanovsky, Model-based plant design and hierarchical control of a prototype lighter-than-air wind energy system, with experimental flight test results, IEEE Transactions on Control Systems Technology 22 (2) (2013) 531–542. doi:10.1109/TCST.2013.2263505.

[64] P. Williams, B. Lansdorp, W. Ockels, Modeling and control of a kite on a variable length flexible inelastic tether, in: AIAA Modeling and Simulation Technologies Conference and Exhibit, 2007, pp. 1–20. doi:10.2514/6.2007-6705.

[65] S. Gros, M. Diehl, Modeling of airborne wind energy systems in natural coordinates, in: U. Ahrens, M. Diehl, R. Schmehl (Eds.), Airborne Wind Energy, Green Energy and Technology, Springer, Berlin Heidelberg, 2013, Ch. 10, pp. 181–203. doi:10.1007/978-3-642-39965-7_10.

[66] D. Eijkelhof, S. Rapp, U. Fasel, M. Gaunaa, R. Schmehl, Reference design and simulation framework of a multi-megawatt airborne wind energy system, Journal of Physics: Conference Series 1618 (2020) 032020. doi:10.1088/1742-6596/1618/3/032020.

[67] N. Bigi, A. Nême, K. Roncin, J.-B. Leroux, G. Bles, C. Jochum, Y. Parlier, Analytical tether model for static kite flight, in: R. Schmehl (Ed.), Airborne Wind Energy – Advances in Technology Development and Research, Green Energy and Technology, Springer, Singapore, 2018, Ch. 3, pp. 57–78. doi:10.1007/978-981-10-1947-0_3.

[68] U. Fechner, R. van der Vlugt, E. Schreuder, R. Schmehl, Dynamic model of a pumping kite power system, Renewable Energy 83 (2015) 705–716. doi:10.1016/j.renene.2015.04.028.

[69] P. Williams, Cable modeling approximations for rapid simulation, Journal of Guidance, Control, and Dynamics 40 (7) (2017) 1779–1788. doi:10.2514/1.G002354.

[70] P. J. Antsaklis, K. M. Passino, S. J. Wang, An introduction to autonomous control systems, IEEE Control Systems Magazine 11 (4) (1991) 5–13. doi:10.1109/37.88585.

[71] R. Chatila, R. Alami, B. Degallaix, H. Laruelle, Integrated planning and execution control of autonomous robot actions, in: Proceedings 1992 IEEE International Conference on Robotics and Automation, Vol. 3, 1992, pp. 2689–2696. doi:10.1109/ROBOT.1992.219999.

[72] M. Pachter, P. R. Chandler, Challenges of autonomous control, IEEE Control Systems Magazine 18 (4) (1998) 92–97. doi:10.1109/37.710883.

[73] E. Balaban, J. J. Alonso, An approach to prognostic decision making in the aerospace domain, in: Annual Conference of the Prognostics and Health Management Society, Vol. 3, Minneapolis, MN, USA, 2012, pp. 1–19.
URL https://c3.nasa.gov/dashlink/resources/879/

[74] S. Jacklin, J. Schumann, P. Gupta, M. Lowry, J. Bosworth, E. Zavala, K. Hayhurst, C. Belcastro, C. Belcastro, Verification, validation, and certification challenges for adaptive flight-critical control system software, in: AIAA Guidance, Navigation, and Control Conference and Exhibit, Providence, Rhode Island, 2012, pp. 1–10. doi:10.2514/6.2004-5258.

[75] P. Koopman, M. Wagner, Autonomous vehicle safety: An interdisciplinary challenge, IEEE Intelligent Transportation Systems Magazine 9 (1) (2017) 90–96. doi:10.1109/MITS.2016.2583491.

[76] W. Schwarting, J. Alonso-Mora, D. Rus, Planning and decision-making for autonomous vehicles, Annual Review of Control, Robotics, and Autonomous Systems 1 (1) (2018) 187–210. doi:10.1146/annurev-control-060117-105157.

[77] C. Jehle, R. Schmehl, Applied tracking control for kite power systems, AIAA Journal of Guidance, Control, and Dynamics 37 (4) (2014) 1211–1222. doi:10.2514/1.62380.

[78] S. Rapp, R. Schmehl, E. Oland, S. Smidt, T. Haas, J. Meyers, A modular control architecture for airborne wind energy systems, in: Proceedings of the AIAA Scitech 2019, San Diego, California, 2019, pp. 1–25. doi:10.2514/6.2019-1419.

[79] S. Rapp, R. Schmehl, E. Oland, T. Haas, Cascaded pumping cycle control for rigid wing airborne wind energy systems, Journal of Guidance, Control, and Dynamics 42 (11) (2019) 2456–2473. doi:10.2514/1.G004246.

[80] S. Diwale, T. Faulwasser, C. N. Jones, Model predictive path-following control for airborne wind energy systems, IFAC-PapersOnLine 50 (1) (2017) 13270–13275.

[81] T. A. Wood, E. Ahbe, H. Hesse, R. S. Smith, Predictive guidance control for autonomous kites with input delay, IFAC-PapersOnLine 50 (1) (2017) 13276–13281.

[82] R. Ruiterkamp, S. Sieberling, Description and preliminary test results of a six degrees of freedom rigid wing pumping system, in: U. Ahrens, M. Diehl, R. Schmehl (Eds.), Airborne Wind Energy, Green Energy and Technology, Springer, Berlin Heidelberg,

2013, Ch. 26, pp. 443–458. doi:10.1007/978-3-642-39965-7_26.

[83] U. Fechner, R. Schmehl, Flight path control of kite power systems in a turbulent wind environment, in: Proceedings of the 2016 American Control Conference (ACC), IEEE, Boston, MA, USA, 2016, pp. 4083–4088. doi:10.1109/ACC.2016.7525563.

[84] F. Holzapfel, G. Sachs, Dynamic inversion based control concept with application to an unmanned aerial vehicle, in: AIAA Guidance, Navigation, and Control Conference and Exhibit, Providence, Rhode Island, 2004, pp. 1–13. doi:10.2514/6.2004-4907.

[85] S. Diwale, A. Alessandretti, I. Lymperopoulos, C. N. Jones, A nonlinear adaptive controller for airborne wind energy systems, in: 2016 American Control Conference (ACC), IEEE, 2016, pp. 4101–4106.

[86] T. A. Wood, H. Hesse, R. S. Smith, Predictive control of autonomous kites in tow test experiments, IEEE control systems letters 1 (1) (2017) 110–115.

[87] E. Ahbe, T. A. Wood, R. S. Smith, Transverse contraction-based stability analysis for periodic trajectories of controlled power kites with model uncertainty, in: 2018 IEEE Conference on Decision and Control (CDC), IEEE, 2018, pp. 6501–6506.

[88] N. Rontsis, S. Costello, I. Lymperopoulos, C. N. Jones, Improved path following for kites with input delay compensation, in: 2015 54th IEEE Conference on Decision and Control (CDC), IEEE, 2015, pp. 656–663.

[89] A. U. Zgraggen, L. Fagiano, M. Morari, Real-time optimization and adaptation of the crosswind flight of tethered wings for airborne wind energy, IEEE Transactions on Control Systems Technology 23 (2) (2015) 434–448.

[90] L. Fagiano, E. Nguyen-Van, F. Rager, S. Schnez, C. Ohler, Autonomous take off and flight of a tethered aircraft for airborne wind energy, IEEE transactions on control systems technology 26 (1) (2018) 151–166. doi:10.1109/TCST.2017.2661825.

[91] M. Behrel, K. Roncin, D. Grelon, F. Montel, A. Nême, J.-B. Leroux, C. Jochum, Y. Parlier, Performance measurement of a 50-square-meter kite set-up on a 13-meter trawler, La Houille Blanche (2019) 67–69doi:10.1051/lhb/2019036.

[92] E. Schmidt, M. De Lellis Costa de Oliveira, R. Saraiva da Silva, L. Fagiano, A. Trofino Neto, In-flight estimation of the aerodynamics of tethered wings for airborne wind energy, IEEE Transactions on Control Systems Technology 28 (4) (2020) 1309–1322.

[93] S. S. Diwale, I. Lymperopoulos, C. N. Jones, Optimization of an airborne wind energy system using constrained gaussian processes, in: 2014 IEEE Conference on Control Applications (CCA), IEEE, 2014, pp. 1394–1399.

[94] S. Rapp, R. Schmehl, Enhancing resilience of airborne wind energy systems through upset condition avoidance, Journal of Guidance, Control, and Dynamics 44 (2) (2021) 251–265. doi:10.2514/1.G005189.

[95] L. Fagiano, K. Huynh, B. Bamieh, M. Khammash, On sensor fusion for airborne wind energy systems, IEEE Transactions on Control Systems Technology 22 (3) (2013) 930–943.

[96] F. Girrbach, J. D. Hol, G. Bellusci, M. Diehl, Optimization-based sensor fusion of gnss and imu using a moving horizon approach, Sensors 17 (5) (2017) 1159.

[97] A. Millane, H. Hesse, T. A. Wood, R. S. Smith, Range-inertial estimation for airborne wind energy, in: 2015 54th IEEE Conference on Decision and Control (CDC), IEEE, 2015, pp. 455–460.

[98] H. Hesse, M. Polzin, T. A. Wood, R. S. Smith, Visual motion tracking and sensor fusion for kite power systems, in: U. Ahrens, M. Diehl, R. Schmehl (Eds.), Airborne Wind Energy – Advances in Technology Development and Research, Green Energy and Technology, Springer, Singapore, 2018, Ch. 17, pp. 413–438. doi:10.1007/978-3-642-39965-7_17.

[99] M. Polzin, T. A. Wood, H. Hesse, R. S. Smith, State estimation for kite power systems with delayed sensor measurements, IFAC-PapersOnLine 50 (1) (2017) 11959–11964.

[100] G. Licitra, S. Sieberling, S. Engelen, P. Williams, R. Ruiterkamp, M. Diehl, Optimal Control for Minimizing Power Consumption During Holding Patterns for Airborne Wind Energy Pumping System, in: Proceedings of the European Control Conference (ECC), 2016, pp. 1574–1579. doi:10.1109/ECC.2016.7810515.

[101] J. Sternberg, J. Goit, S. Gros, J. Meyers, M. Diehl, Robust and stable periodic flight of power generating kite systems in a turbulent wind flow field, in: IFAC Proceedings Volumes (IFAC-PapersOnline), Vol. 45, 2012, pp. 140–145. doi:10.3182/20120913-4-IT-4027.00009.

[102] G. Horn, S. Gros, M. Diehl, Numerical trajectory optimization for airborne wind energy systems described by high fidelity aircraft models, in: U. Ahrens, M. Diehl, R. Schmehl (Eds.), Airborne Wind Energy, Green Energy and Technology, Springer, Berlin Heidelberg, 2013, Ch. 11, pp. 205–218. doi:10.1007/978-3-642-39965-7_11.

[103] G. Licitra, J. Koenemann, A. Bürger, P. Williams, R. Ruiterkamp, M. Diehl, Performance assessment of a rigid wing Airborne Wind Energy pumping system, Energy 173 (2019) 569–585. doi:10.1016/j.energy.2019.02.064.

[104] M. Canale, L. Fagiano, M. Milanese, High altitude wind energy generation using controlled power kites, IEEE Transactions on Control Systems Technology 18 (2) (2010) 279–293. doi:10.1109/TCST.2009.2017933.

[105] M. C. Fernandes, L. Tiago Paiva, F. A. Fontes, Heading angle control for path-following guidance with large domain of attraction of a pumping kite generator, in: Book of Abstracts of the International Airborne Wind Energy Conference 2019, University of Strathclyde, Glasgow, United Kingdom, 2019, p. 87.
URL http://resolver.tudelft.nl/uuid:a9d8f367-f52f-4358-a40e-8bd0977a1a45

[106] M. Aull, A. Stough, K. Cohen, Design Optimization and Sizing for Fly-Gen Airborne Wind Energy Systems, Automation 1 (1) (2020) 1–16. doi:10.3390/automation1010001.
URL https://www.mdpi.com/2673-4052/1/1/1

[107] B. Houska, M. Diehl, Robustness and stability optimization of power generating kite systems in a periodic pumping mode, in: Proceedings of the IEEE Multi-conference on Systems and Control (MSC), Yokohama, Japan, 2010, pp. 2172–2177. doi:10.1109/CCA.2010.5611288.
URL http://ieeexplore.ieee.org/xpls/abs_all.jsp?arnumber=5611288

[108] R. Saraiva, M. De Lellis, A. Trofino, Passive Phase Design of a Pumping Kite Wind Generator, IFAC Proceedings Volumes 47 (3) (2014) 6764–6769, 19th IFAC World Congress. doi:10.3182/20140824-6-ZA-1003.01338.

[109] J. Betts, Practical Methods for Optimal Control and Estimation Using Nonlinear Programming, 2nd Edition, SIAM, 2010.

[110] L. T. Biegler, Nonlinear Programming, MOS-SIAM Series on Optimization, SIAM, 2010.

[111] J. B. Rawlings, D. Q. Mayne, M. M. Diehl, Model Predictive Control: Theory, Computation, and Design, 2nd Edition, Nob Hill, 2017.

[112] J. Koenemann, P. Williams, S. Sieberling, M. Diehl, Modeling of an airborne wind energy system with a flexible tether model for the optimization of landing trajectories, IFAC-PapersOnLine 50 (1) (2017) 11944–11950. `doi:10.1016/j.ifacol.2017.08.1037`.

[113] J. Gillis, J. Goos, Reversed pumping for tethered airplanes in no-wind conditions, in: Book of Abstracts of the International Airborne Wind Energy Conference 2011, Leuven, Belgium, 2011, p. 25.
URL http://resolver.tudelft.nl/uuid:ee654eb5-9d44-4c6b-9f6c-568d5d9648ac

[114] G. Licitra, J. Koenemann, G. Horn, P. Williams, R. Ruiterkamp, M. Diehl, Viability assessment of a rigid wing airborne wind energy pumping system, in: Proceedings of the 2017 21st International Conference on Process Control, PC 2017, Institute of Electrical and Electronics Engineers Inc., 2017, pp. 452–458. `doi:10.1109/PC.2017.7976256`.
URL http://ieeexplore.ieee.org/document/7976256/

[115] E. C. Malz, V. Verendel, S. Gros, Computing the Power Profiles for an Airborne Wind Energy System based on Large-Scale Wind Data, Renewable Energy accepted (2020).

[116] M. Sommerfeld, C. Crawford, Airborne wind energy trajectory optimization using realistic wind speed profiles, in: Wind Energy Science Conference 2019, Cork, Ireland, 2019. `doi:10.5281/zenodo.3357152`.

[117] L. A. Roque, L. T. Paiva, M. C. Fernandes, D. B. Fontes, F. A. Fontes, Layout optimization of an airborne wind energy farm for maximum power generation, Energy Reports 6 (2020) 165–171. `doi:10.1016/j.egyr.2019.08.037`.

[118] E. C. Malz, M. Zanon, S. Gros, A Quantification of the Performance Loss of Power Averaging in Airborne Wind Energy Farms, in: 2018 European Control Conference, ECC 2018, Institute of Electrical and Electronics Engineers Inc., 2018, pp. 58–63. `doi:10.23919/ECC.2018.8550357`.

[119] E. C. Malz, F. Hedenus, L. Göransson, V. Verendel, S. Gros, Drag-mode airborne wind energy vs. wind turbines: An analysis of power production, variability and geography, Energy 193 (2020) 116765. `doi:10.1016/j.energy.2019.116765`.

[120] E. Malz, L. Göransson, S. Gros, The Value of Airborne Wind Energy in a Zero-Emission Electricity System, in: Book of Abstracts of the International Airborne Wind Energy Conference 2019, University of Strathclyde, Glasgow, United Kingdom, 2019, p. 118.
URL http://resolver.tudelft.nl/uuid:9f22348c-8e54-4dd1-85ba-3d14d09b53fd

[121] J. A. E. Andersson, J. Gillis, G. Horn, J. B. Rawlings, M. Diehl, CasADi - A software framework for nonlinear optimization and optimal control, Mathematical Programming Computation 11 (1) (2019) 1–36. `doi:10.1007/s12532-018-0139-4`.
URL http://link.springer.com/10.1007/978-3-642-30023-3{_}27

[122] J. Koenemann, J. De Schutter, R. Leuthold, G. Licitra, M. Diehl, OpenOCL-The Open Optimal Control Library, in: Book of Abstracts of the International Airborne Wind Energy Conference 2019, University of Strathclyde, Glasgow, United Kingdom, 2019, p. 92.
URL http://resolver.tudelft.nl/uuid:f6d99d01-5acd-47ee-848e-18407491c192

[123] G. Sánchez-Arriaga, LAgrangian Kite SimulAtors (LAKSA).
URL https://github.com/apastor3/laksa

[124] J. De Schutter, R. Leuthold, T. Bronnenmeyer, E. Malz, S. Gros, M. Diehl, awebox: Modelling and optimal control of single- and multiple-kite systems for airborne wind energy.
URL https://github.com/awebox/awebox

[125] M. Zanon, S. Gros, J. Meyers, M. Diehl, Airborne Wind Energy: Airfoil-Airmass Interaction, IFAC Proceedings Volumes 47 (3) (2014) 5814–5819, 19th IFAC World Congress. `doi:10.3182/20140824-6-za-1003.00258`.

[126] L. Grüne, J. Pannek, Nonlinear Model Predictive Control, second edition Edition, Springer-Verlag, 2017.

[127] F. Borrelli, A. Bemporad, M. Morari, Predictive control for linear and hybrid systems, Cambridge University Press, 2017.

[128] M. Diehl, Real-time optimization for large scale nonlinear processes, Ph.D. thesis, University of Heidelberg (2001).
URL http://archiv.ub.uni-heidelberg.de/volltextserver/1659/

[129] M. Diehl, H. G. Bock, J. P. Schlöder, A real-time iteration scheme for nonlinear optimization in optimal feedback control, SIAM Journal on Control and Optimization 43 (5) (2005) 1714–1736. `doi:10.1137/S0363012902400713`.
URL http://epubs.siam.org/sicon/resource/1/sjcodc/v43/i5/p1714_s1

[130] M. Canale, L. Fagiano, M. Ippolito, M. Milanese, Control of tethered airfoils for a new class of wind energy generator, in: Proceedings of the 45th IEEE Conference on Decision and Control, IEEE, 2006, pp. 4020–4026.

[131] A. Ilzhoefer, B. Houska, M. Diehl, Nonlinear MPC of kites under varying wind conditions for a new class of large scale wind power generators, International Journal of Robust and Nonlinear Control 17 (17) (2007) 1590–1599. `doi:10.1002/rnc.1210`.
URL http://onlinelibrary.wiley.com/doi/10.1002/rnc.1210/abstract

[132] H. J. Ferreau, B. Houska, K. Geebelen, M. Diehl, Real-time control of a kite-model using an auto-generated nonlinear mpc algorithm, IFAC Proceedings Volumes 44 (1) (2011) 2488–2493.

[133] S. Gros, M. Zanon, M. Diehl, Orbit control for a power generating airfoil based on nonlinear mpc, in: 2012 American Control Conference (ACC), IEEE, 2012, pp. 137–142.

[134] M. Zanon, S. Gros, M. Diehl, Model predictive control of rigid-airfoil airborne wind energy systems, in: U. Ahrens, M. Diehl, R. Schmehl (Eds.), Airborne Wind Energy, Green Energy and Technology, Springer, Berlin Heidelberg, 2013, Ch. 12, pp. 219–233. `doi:10.1007/978-3-642-39965-7_12`.

[135] M. Zanon, G. Horn, S. Gros, M. Diehl, Control of dual-airfoil airborne wind energy systems based on nonlinear MPC and MHE, in: Proceedings of the European Control Conference (ECC), 2014, pp. 1801–1806.

[136] S. Lucia, S. Engell, Control of towing kites under uncertainty using robust economic nonlinear model predictive control, in: 2014 European Control Conference (ECC), IEEE, 2014, pp. 1158–1163.

[137] B. Karg, S. Lucia, Learning-based approximation of robust nonlinear predictive control with state estimation applied to a towing kite, in: 2019 18th European Control Conference (ECC), IEEE, 2019, pp. 16–22.

[138] M. Vukov, S. Gros, G. Horn, G. Frison, K. Geebelen, J. B. Jørgensen, J. Swevers, M. Diehl, Real-time nonlinear MPC and MHE for a large-scale mechatronic application, Control Engineering Practice 45 (2015) 64–78.

[139] B. Houska, H. J. Ferreau, M. Diehl, ACADO toolkit – an open source framework for automatic control and dynamic optimization, Optimal Control Applications and Methods 32 (3) (2011) 298–312. doi:10.1002/oca.939.
URL http://onlinelibrary.wiley.com/doi/10.1002/oca.939/abstract

[140] R. Verschueren, G. Frison, D. Kouzoupis, N. van Duijkeren, A. Zanelli, R. Quirynen, M. Diehl, Towards a modular software package for embedded optimization, IFAC-PapersOnLine 51 (20) (2018) 374–380.

[141] G. Licitra, A. Bürger, P. Williams, R. Ruiterkamp, M. Diehl, Aerodynamic model identification of an autonomous aircraft for airborne wind energy, Optimal Control Applications and Methods 40 (3) (2019) 422–447.

[142] G. Licitra, A. Bürger, P. Williams, R. Ruiterkamp, M. Diehl, Optimal input design for autonomous aircraft, Control Engineering Practice 77 (2018) 15–27.

[143] K. Ariyur, M. Krstic, Real-Time Optimization by Extremum Seeking Control, John Wiley & Sons, Inc., 2003.

[144] A. Bafandeh, C. Vermillion, Altitude optimization of airborne wind energy systems via switched extremum seeking - design, analysis, and economic assessment, IEEE Transactions on Control Systems Technology 25 (6) (2016) 2022–2033. doi:10.1109/TCST.2016.2632534.

[145] M. Kehs, C. Vermillion, H. Fathy, Online energy maximization of an airborne wind energy turbine in simulated periodic flight, IEEE Transactions on Control Systems Technology 26 (2) (2017) 393–403. doi:10.1109/TCST.2017.2665553.

[146] M. Cobb, K. Barton, H. Fathy, C. Vermillion, An iterative learning approach for online flight path optimization for tethered energy systems undergoing cyclic spooling motion, in: 2019 American Controls Conference (ACC), 2019, pp. 2164–2170. doi:10.23919/ACC.2019.8814773.

[147] Kitepower B.V., A 40 square meter success, accessed 30 June 2020 (2018).
URL https://kitepower.nl/a-40-square-meter-success/

[148] E. Bontekoe, Up! How to launch and retrieve a tethered aircraft, Master's thesis, Delft University of Technology (August 2010).
URL http://resolver.tudelft.nl/uuid:0f79480b-e447-4828-b239-9ec6931bc01f

[149] L. Fagiano, S. Schnez, On the take-off of airborne wind energy systems based on rigid wings, Renewable Energy 107 (2015) 473–488. doi:10.1016/j.renene.2017.02.023.

[150] S. Rapp, R. Schmehl, Vertical takeoff and landing of flexible wing kite power systems, Journal of Guidance, Control, and Dynamics 41 (11) (2018) 2386–2400.

[151] K. Hussen, et al., Study on challenges in the commercialisation of airborne wind energy systems, Tech. Rep. PP-05081-2016, prepared by Ecorys BV for the European Commission's DG Research and Innovation, Brussels (September 2018). doi:10.2777/87591.

[152] N. Deodhar, A. Bafandeh, J. Deese, B. Smith, T. Muyimbwa, C. Vermillion, P. Tkacik, Laboratory-scale flight characterization of a multitethered aerostat for wind energy generation, AIAA Journal 55 (6) (2017) 1823–1832. doi:10.2514/1.J054407.

[153] M. Cobb, N. Deodhar, C. Vermillion, Lab-scale experimental characterization and dynamic scaling assessment for closed-loop crosswind flight of airborne wind energy systems, ASME Journal of Dynamic Systems, Measurement, and Control 140 (7) (2018). doi:10.1115/1.4038650.

[154] A. Siddiqui, K. Naik, M. Cobb, K. Granlund, C. Vermillion, Lab-scale, closed-loop experimental characterization, model refinement, and validation of a hydrokinetic energy-harvesting kite, ASME Journal of Dynamic Systems, Measurement, and Control - accepted, awaiting press (2020).

[155] H. J. Ferreau, B. Houska, K. Geebelen, M. Diehl, Real-time control of a kite-model using an auto-generated nonlinear mpc algorithm, IFAC Proceedings Volumes 44 (1) (2011) 2488 – 2493, 18th IFAC World Congress.

[156] M. Rushdi, T. Dief, S. Yoshida, R. Schmehl, Towing test data set of the Kyushu University kite system, Data 5 (3) (2020) 69. doi:10.3390/data5030069.

[157] R. Schmehl (Ed.), Airborne Wind Energy – Advances in Technology Development and Research, Green Energy and Technology, Springer, 2018.

[158] U. Ahrens, M. Diehl, R. Schmehl (Eds.), Airborne Wind Energy, Green Energy and Technology, Springer, 2013.

[159] L. Fagiano, T. Marks, Design of a small-scale prototype for research in airborne wind energy, IEEE/ASME Transactions on Mechatronics 20 (1) (2015) 166–177.

[160] L. Fagiano, E. Nguyen-Van, F. Rager, S. Schnez, C. Ohler, A small-scale prototype to study the take-off of tethered rigid aircrafts for airborne wind energy, IEEE/ASME Transactions on Mechatronics 22 (4) (2017) 1869–1880.

[161] R. van der Vlugt, J. Peschel, R. Schmehl, Design and experimental characterization of a pumping kite power system, in: U. Ahrens, M. Diehl, R. Schmehl (Eds.), Airborne Wind Energy, Green Energy and Technology, Springer, Berlin Heidelberg, 2013, Ch. 23, pp. 403–425. doi:10.1007/978-3-642-39965-7_23.

[162] J. Oehler, R. Schmehl, Aerodynamic characterization of a soft kite by in situ flow measurement, Wind Energy Science 4 (1) (2019) 1–21. doi:10.5194/wes-4-1-2019.

[163] J. Oehler, R. Schmehl, J. Peschel, P. Faggiani, B. Buchholz, Kite power flight data acquired on 24 march 2017, 4TU.Centre for Research Data, Dataset (2018). doi:10.4121/uuid:37264fde-2344-4af2-860c-effda9caa3e8.

[164] M. A. Rushdi, A. A. Rushdi, T. N. Dief, A. M. Halawa, S. Yoshida, R. Schmehl, Power prediction of airborne wind energy systems using multivariate machine learning, Energies 13 (9) (2020) 2367. doi:10.3390/en13092367.

[165] M. Rushdi, R. Schmehl, T. Dief, S. Yoshida, D. Fujimoto, K. Sawano, Towing test data of the Kyushu University kite system, 4TU.Centre for Research Data, Dataset (2020). doi:10.4121/uuid:c3cee766-2804-4c00-924f-8a9f6c8122fc.

[166] Minesto, Ltd.

URL https://www.minesto.com

[167] SeaQurrent Holding BV.
URL https://seaqurrent.com/

[168] D. Olinger, Y. Wang, Hydrokinetic energy harvesting using tethered undersea kites, Journal of Renewable and Sustainable Energy 7 (2015) 1–18. `doi:10.1063/1.4926769`.

[169] M. Diehl, Airborne wind energy: Basic concepts and physical foundations, in: U. Ahrens, M. Diehl, R. Schmehl (Eds.), Airborne Wind Energy, Green Energy and Technology, Springer, Berlin Heidelberg, 2013, Ch. 1, pp. 3–22. `doi:10.1007/978-3-642-39965-7_1`.

[170] M. Landberg, Submersible plant, US Patent 8,246,293. Application PCT/EP2007/; granted August 21, 2012.

[171] H. Yang, H. Park, Y. Lee, The design of combined energy generation using airborne and ocean current kites in offshore, in: IEEE Offshore Energy and Storage Summit (OSES), 2019, pp. 1–5. `doi:10.1109/OSES.2019.8867204`.

[172] D. Laws, B. Epps, Hydrokinetic energy conversion: Technology, research, and outlook, Renewable and Sustainable Energy Reviews 57 (2016) 1245–1259. `doi:10.1016/j.rser.2015.12.189`.

[173] D. Kumar, S. Sarkar, A review on the technology, performance, design optimization, reliability, techno-economics and environmental impacts of hydrokinetic energy conversion systems, Renewable and Sustainable Energy Reviews 58 (2016) 796–813. `doi:10.1016/j.rser.2015.12.247`.

[174] M. Sood, S. Singal, Development of hydrokinetic energy technology: A review, International Journal of Energy Research 43 (2019) 5552–5571. `doi:10.1002/er.4529`.

[175] R. Moodley, M. Nihontho, S. Chowdhury, S. Chowdhury, A technical and economic analysis of energy extraction from the Agulhas current on the east coast of South Africa, in: IEEE Power & Energy Society General Meeting: New Energy Horizons – Opportunities and Challenges, 2012, pp. 1–8. `doi:10.1109/PESGM.2012.6344793`.

[176] A. Ghasemi, D. J. Olinger, G. Tryggvason, A nonlinear computational model of tethered underwater kites for power generation, Journal of Fluids Engineering 138 (12) (2016) 1–10. `doi:10.1115/1.4034195`.

[177] Z. Liu, Y. Zhao, Y. Zhou, F. Guan, Modeling, simulation and test results analysis of tethered undersea kite based on bead model, Renewable Energy 154 (2020) 1314–1326. `doi:10.1016/j.renene.2020.03.013`.

[178] A. Ghasemi, D. J. Olinger, G. Tryggvason, Computational investigation of a full-scale tethered underwater kite, in: Proceedings of POWER & ENERGY Conference & Exhibition 2018, Paper No. PowerEnergy2018-7397, 2018, pp. 1–11. `doi:10.1115/POWER2018-7397`.

[179] A. Ghasemi, Computational modeling of tethered undersea kites for power generation, Ph.D. thesis, Worcester Polytechnic Institute, https://digitalcommons.wpi.edu/etd-dissertations/56 (February 2018).

[180] H. Li, D. J. Olinger, M. Demetriou, Modeling and control of tethered undersea kites, Ocean Engineering 190 (15) (2019) 1–10. `doi:10.1016/j.oceaneng.2019.106390`.

[181] L. Paiva, F. Fontes, Optimal electric power generation with underwater kite systems, Computing 10 (2018) 1137–1153. `doi:10.1007/s00607-018-0643-4`.

[182] J. Daniels, J. Reed, M. Cobb, A. Siddiqui, C. Vermillion, Optimal cyclic spooling control for kite-based energy systems, in: IFAC World Congress, Berlin, Germany, 2020, pp. 1–7.

[183] G. Mademlis, Y. Liu, C. Pelyuan, E. Singhroy, Design of maximum power point tracking for dynamic power response of tidal undersea kite systems, IEEE Transactions on Industry Applications 56 (2) (2020) 2048–2060. `doi:10.1109/TIA.2020.2966189`.

[184] J. Reed, M. Cobb, J. Daniels, A. Siddiqui, M. Muglia, C. Vermillion, Hierarchical control design and performance assessment of an ocean kite in a turbulent flow environment, in: IFAC World Congress, Berlin, Germany, 2020, pp. 1–7.